Research Square

Preprints are preliminary reports that have not undergone peer review.
They should not be considered conclusive, used to inform clinical practice,
or referenced by the media as validated information.

A Nutrient-Sensitive O-GlcNAc Switch on RIPK1 Controls Necroptosis and Tissue Homeostasis

Meng Fu

2239874942@qq.com

Department of Dermatology, Xijing Hospital, Fourth Military Medical University

Chen Zhang

Xijing hospital, Fouth military medical university

Chunying Xiao

Fourth Military Medical University

Peng Wu

Key Laboratory of Resource Biology and Biotechnology in Western China, College of Life Sciences, Northwest University

Xin Luo

Department of Dermatology, Xijing Hospital, Xi'an, Shaanxi, P. R. China.

Kang Li

Department of Dermatology, Xijing Hospital, Fourth Military Medical University

Zheng Wang

Department of Dermatology, Xijing Hospital, Fourth Military Medical University

Pei Qiao

Xijing hospital, Fouth military medical university

Bo Ma

Department of Dermatology, Xijing Hospital, Fourth Military Medical University

Erle Dang

Xijing hospital, The fourth millitary medical university

Riichiro Abe

Division of Dermatology, Niigata University Graduate School of Medical and Dental Sciences
https://orcid.org/0000-0002-7582-8609

Zipeng Cao

Jiang Qiao

Department of Dermatology, Xijing Hospital, Xi'an, Shaanxi, P. R. China.

Gang Wang

Department of Dermatology, Xijing Hospital, Fourth Military Medical University https://orcid.org/0000-0002-5842-8080

Article

Keywords: O-GlcNAcylation, RIPK1, glucose metabolism, nucleolar stress, necroptosis, Stevens–Johnson syndrome, toxic epidermal necrolysis

Posted Date: October 30th, 2026

DOI: https://doi.org/10.21203/rs.3.rs-11175045/v1

License: This work is licensed under a Creative Commons Attribution 4.0 International License.
Read Full License

Additional Declarations:
There is no duality of interest

Tables 1 to 5 are available in the Supplementary Files section.

A Nutrient-Sensitive O-GlcNAc Switch on RIPK1 Controls Necroptosis and Tissue Homeostasis

Chen Zhang[a,*], ChunYing Xiao[a,*], JinPeng Wu[b,*], YiXin Luo[a,*], Kang Li[a], XiuZheng Wang[a], Pei Qiao[a], YuBo Ma[a], ErLe Dang[a], Riichiro Abe[c], ZiPeng Cao[d#], HongJiang Qiao[a#], Gang Wang[a#], and Meng Fu[a#].

[a]*Department of Dermatology, Xijing Hospital, Fourth Military Medical University, Xi'an, 710032, China*

[b]*Key Laboratory of Resource Biology and Biotechnology in Western China, College of Life Sciences, Northwest University, Xi'an 710069, China*

[c]*Division of Dermatology, Niigata University Graduate School of Medical and Dental Sciences, Niigata, 951-8510, Japan*

[d]*Department of Health Education and Management and the Ministry of Education Key Lab of Hazard Assessment, School of Public Health, Fourth Military Medical University, Xi'an, 710032, China*

[*]These authors contributed equally to this work

Corresponding authors: Dr. Meng Fu, Department of Dermatology, Xijing Hospital, Xi'an, P. R. China. E-mail: fumeng@fmmu.edu.cn

Dr. Gang Wang, Department of Dermatology, Xijing Hospital, Xi'an, P. R. China. E-mail: wanggangxjyy@163.com

Dr. Hongjiang Qiao, Department of Dermatology, Xijing Hospital, Xi'an, P. R. China. E-mail: xjhongjiangq@fmmu.edu.cn

Dr. Zipeng Cao, Department of Health Education and Management, The Fourth Military Medical University, Xi'an P. R. China. E-mail: czpeng@fmmu.edu.cn

ABSTRACT

How cells couple metabolic status to programmed cell death remains a fundamental question in biology. Here, we report an O-GlcNAc-based metabolic checkpoint coupling glucose availability to RIPK1-dependent necroptosis. In patients with severe drug-induced skin eruptions, proteomic and metabolomic analyses of patients' skin lesions revealed markedly decreased O-GlcNAc transferase (OGT) levels, altered levels of hexosamine biosynthesis pathway (HBP) metabolites, and the downregulation of glucose transporters. Mechanistically, OGT-mediated O-linked β-N-acetylglucosaminylation (O-GlcNAcylation) of RIPK1 at Ser331 maintains K63-linked ubiquitination at Lys377, which supports the formation of cytoprotective complexes (RIPK1/FADD/caspase-8) and limits the RIPK1–RIPK3 interaction. Loss of this modification enhances binding to the deubiquitinase CYLD, reduces K63 ubiquitination, and drives keratinocyte necroptosis. In an SJS/TEN animal model, pharmacological inhibition of O-GlcNAcase (OGA) with Thiamet G or PugNAc restored RIPK1 O-GlcNAcylation, attenuated skin pathology, and normalized systemic metabolic abnormalities. Conversely, OGT inhibition or a RIPK1 Ser331-mimetic peptide exacerbated disease. Collectively, our findings define a nutrient-sensitive post-translational checkpoint that integrates glucose metabolism with cell death and tissue homeostasis, with broad implications for inflammatory and metabolic disorders.

Keywords*: O-GlcNAcylation, RIPK1, glucose metabolism, nucleolar stress, necroptosis, Stevens–Johnson syndrome, toxic epidermal necrolysis*

Abbreviations:

OGT	O-GlcNAc transferase
O-GlcNAcylation	O-linked β-N-acetylglucosamine (O-GlcNAc) modification
RIPK1	Receptor-interacting protein kinase 1
SJS	Stevens–Johnson syndrome
TEN	Toxic epidermal necrolysis

Public Summary

- O-GlcNAcylation of RIPK1 at Ser331 serves as a metabolic checkpoint coupling glucose sensing to necroptosis.
- Loss of this modification enhances RIPK1–RIPK3 interaction and CYLD-mediated deubiquitination, driving cell death.
- OGA inhibition pharmacologically restores this checkpoint, alleviating tissue and systemic metabolic pathology.

INTRODUCTION

How do cells sense nutrients and translate this information into decisions about life and death? This fundamental question lies at the heart of organismal homeostasis and its disruption underpins a wide range of human diseases. Here, we address this question by uncovering a metabolic checkpoint that couples glucose availability to programmed cell death in the skin.

Stevens–Johnson syndrome (SJS) and toxic epidermal necrolysis (TEN) are life-threatening drug-induced eruptions characterized by widespread keratinocyte death and epidermal detachment [1, 2]. Necroptosis, a form of programmed necrosis, has emerged as a major driver of keratinocyte loss in patients with SJS/TEN, with receptor-interacting protein kinase 1 (RIPK1) serving as a central node in this pathway [3–5]. Multiple cell death checkpoints involving intricate posttranslational modifications including ubiquitination, palmitoylation, and phosphorylation suppress RIPK1 kinase activity [6–8]. However, how nutrient metabolic signals modulate RIPK1-dependent necroptosis in SJS/TEN remain elusive.

Cells rely on conserved nutrient-sensing signaling cascades to convert extracellular glucose into cell fate outputs, coordinating cellular survival and death to maintain tissue homeostasis. O-linked β-N-acetylglucosaminylation (O-GlcNAcylation) is an important posttranslational modification that couples nutrient availability to cellular signaling [9, 10]. It is catalyzed by O-GlcNAc transferase (OGT) using uridine diphosphate N-acetylglucosamine (UDP-GlcNAc), the end product of the hexosamine

biosynthetic pathway (HBP) [11, 12]. HBP integrates glucose and acetyl-CoA metabolism, making O-GlcNAcylation as a direct sensor of the metabolic status. Dysregulated O-GlcNAc signaling has been implicated in immune–inflammatory diseases [13], diabetes [14], cancer [15], cardiovascular diseases [16], and cell death [17, 18], but its role in SJS/TEN has not been explored.

Here, we performed proteomic, O-GlcNAcylomic and nontargeted metabolomic analyses of skin lesions from patients with SJS/TEN to identify a nutrient-sensitive checkpoint that controls keratinocyte necroptosis. We find that impaired HBP flux and nucleolar stress converge to suppress O-GlcNAcylation of RIPK1 at Ser331-a modification that acts as a molecular brake on necroptosis. Mechanistically, this single sugar modification maintains K63-linked ubiquitination at Lys377, promoting a cytoprotective RIPK1/FADD/caspase-8 complex and restricting RIPK1–RIPK3 interaction. Loss of this modification, whether by OGT inhibition or genetic mutation, enhances CYLD recruitment, reduces K63 ubiquitination, and unleashes cell death. Importantly, pharmacological restoration of this checkpoint via O-GlcNAcase (OGA) inhibition rescues tissue pathology and systemic metabolic abnormalities *in vivo*.

Collectively, our findings define a previously unrecognized mechanism by which a sugar modification on a central cell death regulator translates nutrient signals into a cell fate decision-a paradigm with broad implications for understanding how metabolism controls tissue homeostasis, inflammation, and disease.

MATERIALS AND METHODS

Subjects and sample collection

Serum samples were obtained from 7 SJS patients (3 males and 4 females; average age, 36.43 y) and 8 TEN patients (5 males and 3 females; average age, 32.0 y) at the Department of Dermatology in Xijing Hospital. The clinical characteristics are listed in Table 1. Skin lesions and nonskin lesions were excised from 3 patients pathologically diagnosed with SJS/TEN, (Erythema Multiforme, EM), and (maculopapular exanthems, MPE). The samples were incubated with 2.5 mg/ml

dispase (Gibco, NY, USA) for 8 h at 4 °C to separate the epidermis from the dermis. Control skin samples were collected from age- and sex-matched healthy individuals undergoing plastic surgery. In accordance with Declaration of Helsinki, Institutional Review Board approval (IRB number: KY20172030-1) was obtained before the patients and healthy volunteers were enrolled in this study, as illustrated in Table 2.

Smac-mimetic-induced TEN mouse model

As previously described [19, 20], C57BL/6J mice were injected subcutaneously with 100 μl of 2 mg/kg Smac mimetic (SM164) (TargetMol, Houston, TX, USA) or vehicle (12% Captisol). OSMI-1 (1 mg/kg), TMG (20 mg/kg), and PugNAc (10 mg/kg) were administered intraperitoneally, and the RIPK1^{Ser331A}-O-GlcNAc peptide (1 mg/kg) was administered intravenously once daily after the SM164 injection. The mice were euthanized on day three; the skin lesions were photographed, scored, and collected for analysis. Clinical macroscopic criteria (edema, erythema, and epidermal disruption) were scored on a 0–3-point scale (0, absent; 1, mild; 2, moderate; and 3, severe). Total clinical scores were calculated by summing the scores for individual criteria scores. This study was carried out in compliance with the ARRIVE guidelines. All experiments used female mice and were approved by the local ethics committee (AFMU-LA-FJ-022).

Statistical analysis

The data were analyzed using GraphPad Prism 6. Comparisons between two groups were performed using the Mann–Whitney U test or an unpaired two-tailed Student's t test after the verification of normality. Multiple group comparisons were conducted using one–way ANOVA followed by Tukey's post hoc test. Pearson's correlation coefficients were calculated for serum markers. Statistical significance was set at $P < 0.05$. The data are presented as the means±SEMs from at least three independent experiments with triplicate samples, unless indicated otherwise.

RESULTS

OGT is the most downregulated protein in SJS/TEN skin lesions and is linked to necroptosis pathways

We performed a proteomic analysis of TEN lesions to elucidate the mechanisms underlying necroptosis in SJS/TEN. Among the 119 differentially expressed proteins (DEPs) between TEN patients and MPE patients (Fig. 1A), OGT was the most significantly downregulated protein in TEN lesions (Fig. 1B, C). The Kyoto Encyclopedia of Genes and Genomes (KEGG) pathway enrichment analysis revealed that the DEPs were enriched mainly in programmed necrotic cell death pathways (Fig. 1D). Gene set enrichment analysis (GSEA) further confirmed that low OGT expression correlated with necroptosis-related pathways, including TNF-α and IFN-γ signaling (Fig. 1E). An analysis of the STRING database indicated a specific interaction between OGT and RIPK1/RIPK3 (Fig. 1F). In a previously established SJS/TEN cell model [4], glycosylation PCR array using LL-37/Ac2-26-treated keratinocytes identified *OGT* as the most downregulated gene among the glycosylation-related genes (Fig. 1G, H). Western blotting confirmed the time-dependent decrease in OGT levels (Fig. 1I). Overall, OGT expression is significantly reduced in SJS/TEN skin lesions and cell models.

Decreased O-GlcNAcylation correlated with necroptosis activation in SJS/TEN patients and mouse models

To further confirm the close interaction between OGT and necroptosis activation, western blotting, RT–PCR, and IHC showed significantly reduced global O-GlcNAcylated protein and OGT levels, but not OGA levels, in SJS/TEN patients compared with MPE patients or healthy individuals (Fig. 2A, B and Fig. S1A). Consistent with necroptosis activation, SJS/TEN patients presented elevated phosphorylation of RIPK1/RIPK3/MLKL levels (Fig. 2C). Systemic corticosteroid treatment dramatically increased global O-GlcNAcylated protein and OGT levels in TEN patients (Fig. 2D). Compared with non-lesional skin, lesional skin from TEN patients had lower O-GlcNAcylation and OGT levels (Fig. 2E). Similarly, in the

SM164-induced TEN-like mouse model, IHC, RT–PCR, and western blotting confirmed obviously reduced O-GlcNAcylation and OGT levels compared with those in wild-type mice (Fig. 2F, G and Fig. S1B). Collectively, necroptosis is activated when O-GlcNAcylation is attenuated in SJS/TEN lesions.

Nucleolar stress drives OGT downregulation *via* p53

The proteomic analysis, western blotting, and IHC revealed the downregulation of ribosome-related proteins (RPLs and RPs) in SJS/TEN skin lesions (Fig. 3A, B and Fig. S2A–C), which was confirmed in LL-37/Ac2-26-treated keratinocytes (Fig. S2D –E). Ribosomes are generated in nucleoli, membrane-less organelles with a fibrillar center (FC) surrounded by a dense fibrillar component (DFC) layer and an outside granular component (GC) layer [21]. Disturbed ribosomal biogenesis leads to p53 activation by disrupting the murine double minute 2 (MDM2)–p53 interaction, a process termed nucleolar stress [22]. Importantly, p53 activation was found to inhibit OGT expression [23]. Indeed, electron microscopy revealed that compared with control keratinocytes, LL-37/Ac2-26-treated keratinocytes and SJS/TEN human or mouse model skin lesions presented increased numbers of nucleoli and smaller nucleoli (Fig. 3C–E). Immunostaining of the nucleolar markers RPA40 (FC), fibrillarin (FBL, DFC), and nucleophosmin1 (NPM1, GC) followed by structured illumination microscopy (SIM) confirmed that LL-37/Ac2-26-treated keratinocytes exhibited fusion of the nucleoli, where the FC and DFC regions relocated to the nucleolar periphery and surrounded the remnant GC, appearing as unraveled "nucleolar necklaces" (Fig. 3F, G). In addition, we observed segregation of FBL in multiple foci throughout the nucleus and decreased expression levels (Fig. S2F–H). Nucleolin was overexpressed and a portion translocated to the nucleoplasm (Fig. S2F–H). Moreover, LL-37/Ac2-26 treatment increased the association of RPL5 and RPL11 with MDM2 (Fig. 3H), a hallmark of nucleolar stress. These results demonstrate that LL-37/Ac2-26 triggers nucleolar stress in keratinocytes.

5-Ethynyl uridine (EU) *in situ* transcription assays revealed significant decreases in nucleolar (pre-rRNA) and chromatin (pre-mRNA) transcription (Fig. 3I). Consistently, pre-rRNAs and the 18S, 5.8S, and 28S rRNAs were downregulated (Fig. 3J), p53

protein levels were increased (Fig. 3K), and the p53 inhibitor significantly upregulated OGT expression (Fig. S2I), suggesting that LL-37/Ac2-26 triggers nucleolar stress and p53 activation, leading to OGT downregulation.

HBP activity and glucose uptake are attenuated in SJS/TEN

Because UDP-GlcNAc is the essential substrate for OGT [24], nontargeted metabolomics revealed the reduced UDP-GlcNAc and glucosamine-6-phosphate levels in keratinocytes treated with LL-37/Ac2-26, as well as in serum and skin lesions from SJS/TEN patients and mouse models (Fig. S3A–D and S4A–C). The levels of the key HBP enzymes fructose-6-phosphate amidotransferase (GFAT) and glucosamine 6-phosphate N-acetyltransferase 1 (GNA1), but not phosphofructokinase (PFK) or hexokinase (HK), were reduced in treated keratinocytes (Fig. S3E). Glycolytic transporter (GLUT1 and GLUT3) expression and glucose uptake clearly decreased (Fig. S3H, I). GNA1 and GLUT1 levels were also reduced in SJS/TEN patients (Fig. S3F, J) but were restored after systemic corticosteroid treatment (Fig. S3G). Similar reductions were observed in skin lesions from SJS/TEN model mice (Fig. S4D, E). Together, these results provide multifaceted evidence that HBP activity and glucose uptake are impaired in individuals with SJS/TEN, leading to OGT downregulation.

OGT deficiency promotes keratinocyte necroptosis and the inflammatory response

CRISPR-Cas9-mediated OGT knockout (OGT-KO) in HaCaT cells was confirmed by DNA sequencing and western blotting (Fig. S5A–E) [25]. OGT-KO cells exhibited significantly reduced viability and ATP production; increased LDH release, ROS, phosphorylation of RIPK1/RIPK3/MLKL, and inflammatory cytokines (Fig. S5F–O). Similar necroptotic phenotypes were observed in keratinocytes transfected with an *OGT* siRNA or treated with OGT inhibitor OSMI-1 (Fig. S6A–K and S7A–G). These effects could be reversed by additional supplementation with TMG or recombinant OGT protein (Fig. S6C–K and S7A–G). Conversely, OGT overexpression increased cell viability and ATP levels; reduced LDH, ROS, cytokines; and suppressed necroptosis markers (Fig. S8A–J). These data confirm that OGT deficiency promotes

keratinocyte necroptosis and the inflammatory response.

OGT interacts with RIPK1 and promotes its O-GlcNAcylation

RIPK1 is a key node in necroptosis pathway and is modified by posttranslational modifications [26]. RIPK1 O-GlcNAcylation was abundant in healthy human and WT mouse skin but obviously reduced in SJS/TEN lesions and OGT-KO cells (Fig. S9A–C). OGT overexpression dose-dependently reduced RIPK1 protein levels (Fig. S9D), and treatment with a specific OGA inhibitor, Thiamet-G (TMG), shortened the RIPK1 half-life (Fig. S9E), indicating that O-GlcNAcylation reduces RIPK1 protein stability. Computational modeling predicted a stable interaction between OGT and RIPK1 (Fig. S9F–H), and co-IP verified their interaction (Fig. S9I). Cotransfection of Flag-RIPK1 with increasing doses of HA-OGT resulted in dose-dependent increases in global O-GlcNAcylation and RIPK1 O-GlcNAcylation (Fig. S9J). Enzymatically inactive OGT mutants (K908A or K852A) [27] failed to increase RIPK1 O-GlcNAcylation, confirming that OGT enzymatic activity is required for RIPK1 O-GlcNAcylation (Fig. S9K). These data demonstrate that OGT specifically interacts with RIPK1 and promotes its O-GlcNAcylation.

Ser331 is a major O-GlcNAcylation site on RIPK1

Next, we sought to identify the potential O-GlcNAcylation sites on RIPK1 (Fig. 4A). Principal component analysis (PCA) showed clear clustering of LL-37/Ac2-26-treated samples and OGT-OV samples, confirming sample reproducibility (Fig. S10A). The WoLF PSORT analysis predicted that most O-GlcNAcylated proteins localize to the nucleus, cytoplasm, and plasma membrane (Fig. S10B). Label-free quantitative O-GlcNAcylomics identified 690 unique O-GlcNAcylated sites and 321 candidate modified proteins (Fig. 4B), with most proteins containing a single modified site (Fig. 4C). The quantitative analysis showed that OGT treatment significantly upregulated the O-GlcNAcylation of RIPK1 at Ser331 (Fig. 4D, E). Gene Ontology (GO) and KEGG enrichment analyses revealed that O-GlcNAcylated proteins are involved mainly in cell death processes (Fig. 4F, G). WikiPathway and Reactome analyses further confirmed that RIPK1 O-GlcNAcylation at Ser331 is associated with necroptosis signaling (Fig. 4H, I). Integrated proteomic

and O-GlcNAcylomic analyses identified Ser331 of RIPK1 as an upregulated O-GlcNAcylation site; DEPs were enriched in cell death pathways, and PPI network confirmed the OGT–RIPK1 interaction (Fig. S11A–E). These results further confirmed that Ser331 is a major O-GlcNAcylation site on RIPK1 linked to necroptosis signaling.

O-GlcNAcylation of RIPK1 at Ser331 negatively regulates keratinocyte necroptosis

The structure of RIPK1 was predicted by the AlphaFold protein structure database to further verify the O-GlcNAcylation sites on RIPK1, and S331 was labeled with a black sphere (Fig. 5A). MS/MS and sanger sequencing confirmed RIPK1 O-GlcNAcylation at Ser331 (Fig. 5B, C). Compared with the WT RIPK1, RIPK1 S331A mutant exhibited significantly reduced O-GlcNAcylation (Fig. 5D–F). OSMI-1 expression was reduced, and TMG increased the O-GlcNAcylation of WT RIPK1 but had no effect on RIPK1 S331A mutant (Fig. 5G). A customized Ser331 O-GlcNAc-specific antibody confirmed OGT-mediated O-GlcNAcylation at this site (Fig. 5H, I). Additionally, the levels of RIPK1–RIPK3 complex and RIPK1 phosphorylation decreased following OGT treatment (Fig. 5J, K). Notably, compared with WT RIPK1, RIPK1 S331A mutant showed enhanced binding to RIPK3 (Fig. 5L, M). Reconstitution of OGT-KO cells with RIPK1 S331A exacerbated necroptosis, inflammation, and phosphorylation of RIPK1/RIPK3/MLKL (Fig. S12A–I). Glucose supplementation increased RIPK1 Ser331 O-GlcNAcylation, whereas glucose uptake inhibition reduced the level of this modification (Fig. S12J, K). Collectively, Ser331 is a key O-GlcNAcylation site on RIPK1 that negatively regulates necroptosis.

Ser331 O-GlcNAcylation modulates the formation of RIPK1/FADD/Caspase-8 complex and K63-linked ubiquitination

Accumulating evidence has shown that O-GlcNAcylation regulates protein–protein interactions [28, 29]. We investigated whether RIPK1 O-GlcNAcylation regulated the formation of RIPK1/FADD/Caspase-8 complex. OSMI-1, OGT-KO and S331A mutation each reduced this complex formation (Fig. 6A–C). OGT deficiency or S331A mutation reduced RIPK1 ubiquitination (Fig. 6D–G). Several types of

ubiquitination have been identified in RIPK1, including K11-, K48-, and K63-linked ubiquitination [30]. Ubiquitination assays revealed that OSMI-1, OGT-KO, and RIPK1 S331A specifically reduced K63-linked (but not K48-linked) RIPK1 ubiquitination (Fig. 6H, I). Among the 4 predicted ubiquitination sites (Lys302, Lys306, Lys316, and Lys377) within the intermediate domain (ID) of RIPK1, only K377R mutation effectively inhibited S331A-induced RIPK1 deubiquitination (Fig. 6J–L), indicating that Lys377 is the key K63-linked ubiquitination site regulated by Ser331 O-GlcNAcylation.

A proteomic analysis of cells expressing RIPK1 WT or S331A mutant showed the downregulaion of E3 ligase TRAF2 and upregulation of the deubiquitinase CYLD (Fig. S13A, B), with Reactome pathway annotations highlighting enrichment of antiapoptotic signaling (Fig. S13C). Co-IP confirmed that OSMI-1, OGT-KO, or S331A mutation enhanced RIPK1–CYLD interaction and reduced RIPK1–TRAF2/cIAP2 interaction (Fig. S13D–G). Collectively, OGT-mediated O-GlcNAcylation of RIPK1 at Ser331 promotes its K63-linked ubiquitination by suppressing the binding of CYLD and decreasing the interaction between RIPK1 and TRAF2/cIAP2.

RIPK1 S331 O-GlcNAcylation suppresses the intermediate domain-mediated RIPK1–RIPK3 interaction and kinase activation

Ser331 is highly conserved across mammals and is located within the ID of RIPK1 (Fig. 7A, B). Reconstitution with RIPK1 S331A increased phosphorylation levels of RIPK1/MLKL (Fig. 7C). The overexpression of WT OGT, but not OGT enzyme-dead mutants (K908A and H508A) [31], abolished RIPK1–RIPK3 heterodimeric interaction, RIPK1–RIPK1 homodimeric interaction, and RIPK1 phosphorylation (Fig. 7D, E). The expression of RIPK1 S331A mutation reversed these effects (Fig. 7F) and rendered RIPK1 resistant to OGT-mediated inhibition of phosphorylation and RIPK3 interaction (Fig. 7F). Deletion mutants of RIPK1 (ΔDI, ΔKI, ΔD) presented defects in RIPK1–RIPK3 interaction and RIPK1 phosphorylation (Fig. 7G, H), but RIPK1 kinase-dead mutants (K45A and D138N) [32] still interacted with RIPK3 (Fig. 7I), indicating that the ID of RIPK1 mediated RIPK1–RIPK3 interaction, which precedes

RIPK1 phosphorylation.

We examined whether RIPK1 S331A-induced hypernecroptotic responses were dependent on the ID of RIPK1 and/or its kinase activity. Both the S331A+ΔID mutant of RIPK1 or S331A/D138N double mutant lacked RIPK1 phosphorylation (Fig. 7J) and abolished the increased necroptotic response (Fig. S14A–C) and cytokine production (Fig. S14D, E) compared with cells reconstituted with RIPK1 S331A. These findings confirm that loss of Ser331 O-GlcNAcylation increases necroptosis via protein–protein interactions mediated by ID of RIPK1 and subsequent RIPK1 kinase activation.

Molecular dynamics simulations reveal conformational changes upon Ser331 O-GlcNAcylation

Molecular dynamics simulations showed that S331A mutation had minimal effects on the main chain stability of RIPK1 (Fig. S15A). The RMSD of RIPK1(WT) and RIPK1(Ala) remains fairly low, with values less than 0.2 nm. The RMSDs of RIPK1 (O-GlcNAc) fluctuated throughout the simulation time, and the values were still greater than 1.0 nm, which indicated that significant conformational changes occurred upon the introduction of O-GlcNAcylation at Ser331 (Fig. S15B). In the RIPK1 (O-GlcNAc)-RIPK3 model, the region spanning residues 624–640 of RIPK1 underwent a conformational downward shift, resulting in a reduction in the binding pocket formed by residues 313–321 and 624–640. This region has been previously reported to interact with SQSTM1 [33], suggesting that this structural alteration may impair SQSTM1 binding and thereby inhibit the interaction of RIPK1 with RIPK3 (Fig. S15C).

OGA inhibition alleviates TEN severity *in vivo* and improves metabolic parameters

We evaluated the efficacy of an intraperitoneal injection of O-GlcNAcase enzyme inhibitor in mouse models of TEN to explore the clinical relevance of our findings. In SM164-induced TEN mouse model, intraperitoneal injection of OGA inhibitor, TMG and PugNAc successfully reduced disease severity on day 3, whereas OSMI injection exacerbated the pathology (Fig. 8A–E and Fig. S16A, B). TMG/PugNAc

353 treatment decreased cutaneous p-RIPK1, RIPK3 and p-MLKL levels (Fig. 8F–H and
354 Fig. S16C), reduced serum IL-6/TNF-α levels (Fig. S16D, E), decreased the size of
355 the spleens (Fig. 8I), decreased keratinocyte death ($TUNEL^+$) and $CD3^+$ immune cell
356 infiltration, and promoted $Ki67^+$ epidermal recovery (Fig. S16H, I). Importantly, liver
357 injury and abnormal glucose levels are closely associated with the pathogenesis of
358 SJS/TEN [2, 34]. The data showed that TMG/PugNAc treatment reduced the serum
359 levels of liver/kidney injury biomarkers (alanine aminotransferase (ALT), aspartate
360 aminotransferase (AST), LDH, creatine kinase isoenzyme (CK-MB)) and normalized
361 glucose levels (Fig. 8J and Fig. S16F, G). In contrast, the administration of RIPK1
362 Ser331A O-GlcNAc peptide exacerbated disease severity; increased the expression of
363 necroptosis markers, splenomegaly, and serum injury markers; and further increased
364 glucose levels (Fig. S17A–M). These data establish that RIPK1 Ser331
365 O-GlcNAcylation is a key regulator of SJS/TEN pathology and support that
366 pharmacological enhancement of O-GlcNAcylation via OGA inhibition ameliorates
367 both skin inflammation and systemic metabolic disturbances.
368

369 # DISCUSSION

370 How cells integrate metabolic status with programmed cell death decisions is a
371 fundamental question in biology. Here, we provide an answer by uncovering a
372 nutrient-sensitive post-translational checkpoint that couples glucose availability to
373 RIPK1-dependent necroptosis. We show that O-GlcNAcylation of RIPK1 at Ser331
374 acts as a molecular brake on necroptosis, and that loss of this modification—driven by
375 impaired HBP flux or nucleolar stress—unleashes cell death and tissue inflammation.
376 This work establishes a direct link between glucose metabolism, protein glycosylation,
377 and cell death signaling, with broad implications for understanding how metabolism
378 controls cell fate in health and disease.

379 Epidermal homeostasis requires a tightly regulated balance between cell survival
380 and death. In severe drug eruptions such as SJS/TEN, this balance is disrupted by
381 massive keratinocyte necroptosis [1]. While immune-derived cytokines such as

TNF-α and IFN-γ are known triggers [2], the intracellular metabolic disturbances that license RIPK1-dependent necroptosis in keratinocytes have remained unexplored. In this study, we identify a previously unrecognized metabolic checkpoint in which glucose flux through the HBP controls O-GlcNAcylation of RIPK1 at Ser331, thereby preventing aberrant necroptosis and maintaining epidermal integrity. Disruption of this checkpoint—by impaired HBP activity or nucleolar stress—derepresses RIPK1, increases necroptosis, and exacerbates inflammatory responses (Fig. 9). Our findings establish pharmacological restoration of the checkpoint via OGA inhibition not only rescues skin pathology but also normalises systemic metabolic parameters, highlighting the therapeutic opportunity of targeting this glycosylation switch.

Abnormalities in O-GlcNAcylation are closely related to the occurrence of necroptosis [15, 17]. Based on this information, we performed integrated proteomic and O-GlcNAcylomic analyses and observed a significant reduction in O-GlcNAcylation levels and OGT expression in SJS/TEN skin lesions and in LL-37/Ac2-26-treated keratinocytes, suggesting a failure of cytoprotective glycosylation mechanisms under causative drug-induced stress response. Importantly, the reductions in O-GlcNAcylation and OGT expression in SJS/TEN skin lesions and their restoration following corticosteroid therapy indicate that monitoring O-GlcNAcylation levels may provide insights into disease activity. In addition, the reduction in O-GlcNAcylation correlated with increased expression of necroptotic markers. These data support the hypothesis that O-GlcNAcylation serves as a metabolic checkpoint that restrains the inappropriate activation of necroptosis in keratinocytes.

A key conceptual advance of this study is the identification that SJS/TEN lesions exhibit profound metabolic dysfunction, specifically in glucose utilization and HBP activity. The HBP converts fructose-6-phosphate to UDP-GlcNAc [35]. Importantly, glucosamine-6-phosphate deficiency is a possible risk factor for the development of SJS/TEN [36, 37]. We found that UDP-GlcNAc and glucosamine-6-phosphate levels are markedly reduced in patients' skin and serum, samples accompanied by decreased expression of the rate-limiting enzymes GFAT and GNA1 as well as the glucose

transporters GLUT1/GLUT3. Given that the availability of UDP-GlcNAc directly regulates OGT activity [11], this metabolic dysregulation contributes to the reduction in O-GlcNAcylation observed in diseased tissues. Notably, TNF-α, which is abundant in SJS/TEN lesions, is known to inhibit glucose transport [38, 39], suggesting the possibility of a feed-forward loop in which inflammation exacerbates metabolic compromise and further suppresses O-GlcNAc signaling. These findings provide a novel perspective on SJS/TEN as a disease involving not only immune dysregulation but also profound metabolic disturbances of the epidermis.

Mechanistically, we identified that nucleolar stress serves as a driver of OGT downregulation in SJS/TEN. Ribosome biogenesis is highly sensitive to the cellular energy status and stress signals [40]. We observed fragmentation of the nucleoli, reduced rRNA transcription, and translocation of nucleolar proteins. These changes led to the increased binding of RPL5/RPL11 to MDM2, p53 activation, and the subsequent transcriptional repression of OGT. These results suggest that drug-induced nucleolar stress may initiate a signaling cascade culminating in OGT downregulation and the subsequent promotion of RIPK1-dependent necroptosis, linking ribosome dysfunction—a classical metabolic stress response—directly to the O-GlcNAcylation machinery. This pathway represents a novel paradigm for determining how drug exposure may trigger disease.

In support of these results, we identified RIPK1 as a direct OGT substrate, with the major modification site localized to Ser331 in its intermediate domain. The loss of S331A significantly reduced the O-GlcNAcylation signal of RIPK1, enhanced RIPK1–RIPK3 interaction, and promoted keratinocyte necroptosis, indicating that O-GlcNAcylation at this site acts as a brake on necroptotic signaling. At the molecular level, O-GlcNAcylation at Ser331 maintained the K63-linked ubiquitination of RIPK1 at Lys377—a modification that stabilizes cytoprotective complexes and restrains kinase activation [41]. Conversely, the loss of O-GlcNAcylation promoted recruitment of the deubiquitinase CYLD, reduced K63-linked ubiquitination, disrupted the formation of RIPK1/FADD/caspase-8 complex. These data establish a direct crosstalk between O-GlcNAcylation and ubiquitination of RIPK1, positioning

OGT as a gatekeeper that couples metabolic status to necroptosis machinery. Molecular dynamics simulations provided additional insights into how Ser331 glycosylation induces conformational changes in the ID, potentially hindering the access of CYLD to Lys377. This dual regulation—metabolic sensing through O-GlcNAc and effector function through ubiquitination—represents a paradigm for how nutrient signals control cell death.

These therapeutic implications are underscored by our *in vivo* experiments. Previous studies have demonstrated that increasing O-GlcNAcylation through TMG protects the cardiovascular system from damage resulting from sepsis[42]. In our study, pharmacological inhibition of OGA with TMG or PugNAc increased RIPK1 O-GlcNAcylation, reduced cutaneous expression of necroptosis markers, and attenuated skin pathology in an SM164-induced TEN mouse model. These treatments also normalized elevated blood glucose and serum liver enzyme levels, indicating that the metabolic benefits extend beyond the skin. In contrast, OSMI-1, an OGT inhibitor, exacerbated disease, underscoring the importance of maintaining O-GlcNAc homeostasis. Importantly, the administration of a RIPK1 Ser331 O-GlcNAc peptide exacerbated pathology, further supporting the functional relevance of this specific modification. Notably, TMG and PugNAc are already under investigation in other disease contexts, and repurposing them for SJS/TEN could accelerate clinical translation.

Several limitations should be acknowledged. First, while we identified Ser331 as a major O-GlcNAcylation site on RIPK1, we cannot exclude the possibility that other residues also contribute to the observed effects. Second, although our mouse model recapitulates key features of TEN, it does not fully capture the complexity of drug-specific, immune-driven pathogenesis in humans. Third, the interplay between HBP metabolism and O-GlcNAcylation in other cell types involved in SJS/TEN pathogenesis warrants further investigation. Future studies using human skin equivalents or patient-derived organoids may provide additional insights.

In summary, our work reveals a metabolic checkpoint in which O-GlcNAcylation of RIPK1 at Ser331 couples glucose availability and nucleolar function to necroptotic

cell death. This checkpoint normally restrains inappropriate cell death, preserving tissue homeostasis. In SJS/TEN, HBP dysfunction and nucleolar stress disable the checkpoint, unleashing necroptosis and inflammation. OGA inhibition represents a conceptually novel approach to treating severe drug-induced eruptions and, potentially, other inflammatory diseases driven by necroptosis. Beyond the therapeutic implications, this study provides a paradigm for how nutrient signals are translated into cell fate decisions through post-translational modification crosstalk—a principle that may extend to many other tissues and disease contexts.

RESOURCE AVAILABILITY

LEAD CONTACT

Further information and requests for resources and reagents should be directed to and will be fulfilled by the lead contact, Meng Fu (fumeng@fmmu.edu.cn).

AVAILABILITY OF MATERIALS

Custom reagents generated in this study include the anti-RIPK1 Ser331-O-GlcNAc antibody and RIPK1 S331A mutant plasmid, which are available from the lead contact upon request under a material transfer agreement.

DATA AND CODE AVAILABILITY

- Any additional information needed to reanalyze the data reported in this paper is available from the lead contact upon reasonable request.
- The mass spectrometry proteomics data have been deposited to the ProteomeXchange Consortium (https://proteomecentral.proteomexchange.org) via the iProX partner repository with the dataset identifier PXD078244. The RNA sequencing data have been deposited to the National genomics data center (https://ngdc.cncb.ac.cn/) with the dataset identifier PRJCA064075.

ACKNOWLEDGEMENTS

The authors thank Le Ma from PTM Bio, Inc., for providing technical assistance. We thank the Analysis & Testing Laboratory for Life Sciences and Medicine of Fourth Military Medical University for performing live imaging.

FUNDING

This study was supported by the National Natural Science Foundation of China (Grant Nos. 82373472 (C.Z.), 82674563 (C.Z.) and 82573994 (M.F.) and the Xijing Hospital Innovative and Special Medical Research Project XJZT26CX34 (C.Z.).

AUTHOR CONTRIBUTIONS

C. Z., C.Y.X., J. P. W., and Y.X.L performed the experiments and processed the samples; X.Z.W., K.L., and P.Q conducted the clinical investigations; E.L.D., and Y.B.M performed the bioinformatics analyses; R.A., Z.P.C., H.J.Q., G.W., and M.F designed the study and wrote the manuscript.

COMPETING INTERESTS

The authors have no relevant conflicts of interest to declare.

ETHICS APPROVAL

Human subject was approved by Ethics Committee of the First Affiliated Hospital of Fourth Military Medical University (IRB number: KY20172030-1). All animal experiments were conducted in accordance with ethical guidelines approved by the Fourth Military Medical University located in Xi'an, China. under the approval number (SYXK(Shaanxi)-20250171).

REFERENCES

1. Gibson A, Deshpande P, Campbell CN, Krantz MS, Mukherjee E, Mockenhaupt M, et al. Updates on the immunopathology and genomics of severe cutaneous adverse drug reactions. J Allergy Clin Immunol. 2023;151(2):289–300.
2. Hasegawa A, Abe R. Stevens-Johnson syndrome and toxic epidermal necrolysis: Updates in pathophysiology and management. Chin Med J (Engl). 2024; 137(19):2294–2307.
3. Saito N, Qiao H, Yanagi T, Shinkuma S, Nishimura K, Suto A, et al. An annexin A1-FPR1 interaction contributes to necroptosis of keratinocytes in severe cutaneous adverse drug reactions. Sci Transl Med. 2014;6(245):245ra95.
4. Kinoshita M, Ogawa Y, Hama N, Ujiie I, Hasegawa A, Nakajima S, et al.

Neutrophils initiate and exacerbate Stevens-Johnson syndrome and toxic epidermal necrolysis. Sci Transl Med. 2021;13(600):eaax2398.

5. Yuan JY, Ofengeim D. A guide to cell death pathways. Nat Rev Mol Cell Biol. 2023;25(5):379–395.
6. Huyghe J, Priem D, Bertrand MJM. Cell death checkpoints in the TNF pathway. Trends Immunol. 2023;44(8):628–643.
7. Varfolomeev E, Vucic D. RIP1 post-translational modifications. Biochem J. 2022;479(9):929–951.
8. Zhang N, Liu J, Guo R, Yan L, Yang Y, Shi C, et al. Palmitoylation licenses RIPK1 kinase activity and cytotoxicity in the TNF pathway. Mol Cell. 2024;84(22):4419–4435.
9. Zhao Q, Zhou S, Lou W, Qian H, Xu Z. Crosstalk between O-GlcNAcylation and phosphorylation in metabolism: regulation and mechanism. Cell Death Differ. 2025;32(7):1181–1199.
10. Ye L, Ding W, Xiao D. Jia Y, Zhao Z, Ao X, et al. O-GlcNAcylation: cellular physiology and therapeutic target for human diseases. MedComm. 2023;4(6):e456.
11. Wang A, Young M, Jiang J. The Glyco-Switch of life: O-GlcNAcylation in cell fate decision. Glycobiology. 2025;35(11):cwaf061.
12. Dupas T, Lauzier B, McGraw S. O-GlcNAcylation: the sweet side of epigenetics. epigenetics chromatin. 2023;16(1):49.
13. Ran Z, Chen C, Ou J. Wu G, Yang C, Liu X. Protein O-GlcNAcylation in health and diseases. MedComm. 2025;6(12):e70536.
14. Naseri R., Navabi SJ, Samimi Z. Mishra AP, Nigam M, Chandra H, et al. Targeting glycoproteins as a therapeutic strategy for diabetes mellitus and its complications. Daru. 2020;28(1):333–358.
15. He XF, Hu X, Wen GJ, Wang Z, Lin WJ. O-GlcNAcylation in cancer development and immunotherapy. Cancer Lett. 2023;566:216258.
16. Malik SS, Pi X, Xie L. O-GlcNAcylation as a Metabolic integrator in cardiovascular physiology and disease. Int J Mol Sci. 2026;27(11):4662.

17. Zhang BC, Li MD, Yin RN. Liu Y, Yang Y, Mitchell-Richards KA, et al. O-GlcNAc transferase suppresses necroptosis and liver fibrosis. JCI Insight. 2019;4(21):e127709.
18. Zhou X, Wang Y, Li X. Zhou J, Yang W, Wang X, et al. O-GlcNAcylation regulates the stability of transferrin receptor (TFRC) to control the ferroptosis in hepatocellular carcinoma cells. Redox Biol. 2024;73:103182.
19. Anderton H, Rickard JA, Varigos GA. Lalaoui N, Silke J. Inhibitor of Apoptosis Proteins (IAPs) Limit RIPK1-Mediated Skin Inflammation. J Invest Dermatol. 2017;137(11):2371–2379.
20. Nordmann .M, Anderton H, Hasegawa A, Schweizer L, Zhang P, Stadler PC, et al. Spatial proteomics identifies JAKi as treatment for a lethal skin disease. Nature. 635(8040):1001–1009.
21. Zhang Y, Lu H. Signaling to p53: ribosomal proteins find their way. Cancer Cell. 2009;16(5):369–377.
22. Yang K, Yang J, Yi J. Nucleolar Stress: hallmarks, sensing mechanism and diseases. Cell Stress. 2018;2(6):125-140.
23. You Z, Peng D, Cao Y, Zhu Y, Yin J, Zhang G, et al. P53 suppresses the progression of hepatocellular carcinoma via miR-15a by decreasing OGT expression and EZH2 stabilization. J Cell Mol Med. 2021;25(19):9168–9182.
24. Liu X, Cai YD, Chiu JC. Regulation of protein O-GlcNAcylation by circadian, metabolic, and cellular signals. J Biol Chem. 2024;300(2):105616.
25. Shafi R, Iyer SP, Ellies LG. O'Donnell N, Marek KW, Chui D, et al. The O-GlcNAc transferase gene resides on the X chromosome and is essential for embryonic stem cell viability and mouse ontogeny. Proc Natl Acad Sci U S A. 2000;97(11):5735–9.
26. Meng Y, Sandow JJ, Czabotar PE. Murphy JM. The regulation of necroptosis by post-translational modifications. Cell Death Differ. 2021;28(3):861–883.
27. Clarke AJ, Hurtado-Guerrero R, Pathak S. Schüttelkopf AW, Borodkin V, Shepherd SM, et al. Structural insights into mechanism and specificity of O-GlcNAc transferase. EMBO J. 2008;27(20):2780–8.

590 28. Yang XY, Qian K. Protein O-GlcNAcylation: emerging mechanisms and
591 functions. Nat Rev Mol Cell Biol. 2017;18(7):452–465.
592 29. Chen Y, Wan R, Zou Z. Lao L, Shao G, Zheng Y, et al. O-GlcNAcylation
593 determines the translational regulation and phase separation of YTHDF proteins.
594 Nat Cell Biol. 2023;25(11):1676–1690.
595 30. Kist M, Kőműves LG, Goncharov T, Dugger DL, Yu C, Roose-Girma M, et al.
596 Impaired RIPK1 ubiquitination sensitizes mice to TNF toxicity and
597 inflammatory cell death. Cell Death Differ. 2020;28(3):985–1000.
598 31. Lazarus MB, Nam Y, Jiang J. Sliz P, Walker S. Structure of human O-GlcNAc
599 transferase and its complex with a peptide substrate. Nature.
600 2011;469(7331):564–7.
601 32. McQuade T, Cho Y, Chan FK. Positive and negative phosphorylation regulates
602 RIP1-and RIP3-induced programmed necrosis. Biochem J. 2013;456(3):409–15.
603 33. Sanz L, Sanchez P, Lallena MJ. Diaz-Meco MT, Moscat J. The interaction of
604 p62 with RIP links the atypical PKCs to NF-kappaB activation. EMBO J.
605 1999;18(11):3044–53.
606 34. Teschke R. Liver Injury in immune Stevens-Johnson Syndrome and Toxic
607 Epidermal Necrolysis: Five New Classification Types. J Clin Transl Hepatol.
608 2025;13(4):339–357.
609 35. Lam C, Low JY, Tran PT. Wang H. The hexosamine biosynthetic pathway and
610 cancer: current knowledge and future therapeutic strategies. Cancer Lett.
611 2021;503:11–18.
612 36. Namazi MR. Glucose-6-phosphate-dehydrogenase deficiency is a possible risk
613 factor for the development of toxic epidermal necrolysis. Med Hypotheses.
614 2007;68(2):466–7.
615 37. Roy Choudhury A, Gadaga C, Moodley L, Moodley A. Metformin-induced
616 hemolysis in a patient with glucose-6-phosphate dehydrogenase deficiency
617 presenting with concurrent idiopathic Steven-Johnson Syndrome/Toxic
618 Epidermal Necrolysis. Cureus. 2021;13(10):e18506.
619 38. Fung KP, Lam WP, Choy YM. et al. Human tumour necrosis factor-alpha

620 inhibits glucose transport in cultured Ehrlich ascites tumour cells. Life Sci.
621 1995;57(1):PL1–6.
622 39. Pincus SH, Kyro A, Maresh GA. Peters T, Kempa J, Marcotte TK, et al.
623 Parenteral exposure of mice to ricin toxin induces fatal hypoglycemia by
624 cytokine-mediated suppression of hepatic glucose-6-phosphatase expression.
625 Toxins (Basel). 2022;14(12):820.
626 40. Noller HF. The ribosome comes to life. Cell. 2024;187(23):6486–6500.
627 41. Li H, Kobayashi M, Blonska M. You Y, Lin X. Ubiquitination of RIP is
628 required for tumor necrosis factor alpha-induced NF-kappaB activation. J Biol
629 Chem. 2006;281(19):13636–13643.
630 42. Ferron M, Cadiet J, Persello A, Prat V, Denis M, Erraud A, et al. O-GlcNAc
631 stimulation: A new metabolic approach to treat septic shock. Sci Rep.
632 2019;9(1):18751.

633

634 FIGURE LEGENDS

635 **Fig. 1 OGT is downregulated in SJS/TEN skin lesions and correlates with**
636 **necroptosis pathways. (A)** Bar chart quantifying DEPs in skin lesions from SJS/TEN
637 patients, MPE patients, and healthy control tissues. **(B)** Volcano plot depicting
638 changes in protein abundance changes in SJS/TEN lesions. **(C)** Heatmap of the
639 hierarchical clustering of DEPs. **(D)** KEGG pathway enrichment analysis. TM:
640 SJS/TEN VS MPE; TN: SJS/TEN VS Normal. **(E)** GSEA results linking low OGT
641 expression with necroptosis-related pathways. **(F)** The protein–protein network was
642 analyzed with the STRING database. **(G)** Volcano plot showing significant
643 differences in mRNA glycosylation and **(H)** KEGG pathway enrichment analysis of
644 differentially expressed genes. **(I)** Time-dependent decrease of total O-GlcNAcylation
645 and OGT.

646 **Fig. 2 Impaired O-GlcNAcylation signaling in patients and mouse models with**
647 **SJS/TEN. (A)** Western blots showing the levels of total O-GlcNAcylation, OGT, and
648 OGA in skin lesions from TEN patients. **(B)** Total O-GlcNAcylation and OGT

649 immunostaining. *Bar* = 100 μm. **(C)** Western blots showing necroptosis-related
650 protein expression in TEN lesions. **(D)** O-GlcNAcylation and OGT levels in TEN
651 lesions before and after treatment with systemic corticosteroids or **(E)** in skin lesions
652 and non-lesional skin from TEN patients. **(F)** Western blots and **(G)** immunostaining
653 showing the total O-GlcNAcylation and OGT levels in an SM164-induced TEN-like
654 mouse model. *Bar* = 100 μm. *ns*, not significant. *$P < 0.05$, **$P < 0.01$, and ***$P <$
655 0.001.
656 **Fig. 3 Nucleolar stress is evident in SJS/TEN skin lesions and cell models. (A)**
657 Volcano plot depicting changes in protein abundance in SJS/TEN lesions compared
658 with MPE lesions and healthy control tissues. **(B)** KEGG pathway enrichment
659 analysis. **(C–E)** SJS/TEN lesions and keratinocytes were treated with LL-37/Ac2-26
660 and observed using TEM. *Bar* = 200 nm. **(F–G)** Keratinocytes were subjected to
661 immunostaining followed by SIM. *Bar* = 50 μm. **(H)** Immunoprecipitated with an
662 anti-MDM2 antibody and detected with anti-RPL5 and anti-RPL11 antibodies. **(I)**
663 Representative images of the EU assay and fluorescence intensity values. *Bar* = 50
664 μm. **(J)** The expression of pre-rRNAs and 18S, 5.8S, and 28S rRNAs was determined
665 using RT–PCR (n = 5). **(K)** Western blots showing the expression level of p53. *ns*, not
666 significant. **$P < 0.01$, and ***$P < 0.001$.
667 **Fig. 4 Overview of the proteins and peptides modified by O-GlcNAcylation. (A)**
668 Flowchart for the enrichment and identification of O-GlcNAcylated peptides by a
669 proteomic analysis. **(B)** Summary of the O-GlcNAcylated peptides and proteins
670 identified across all samples; conserved O-GlcNAcylation motifs are shown. **(C)**
671 Numerical distribution of modified sites. Volcano plot **(D)** and Heatmap **(E)** showing
672 differentially expressed O-GlcNAcylated proteins. GO **(F)** and KEGG pathway **(G)**
673 enrichment analyses of differentially expressed O-GlcNAcylated proteins. Circos
674 plots of regulated-WikiPathway **(H)** and Reactome pathway annotations **(I)**. n=3
675 technical replicates per group.
676 **Fig. 5 RIPK1 O-GlcNAcylation at Ser331 inhibits the RIPK1–RIPK3 interaction.**
677 **(A)** AlphaFold-predicted structure of RIPK1 with Ser331 (black sphere) localized to
678 the intermediate domain (ID). **(B)** MS/MS spectrum confirming the O-GlcNAcylation

of RIPK1 at Ser331. **(C)** Construction of the $RIPK1^{WT}$ and $RIPK1^{S331A}$ mutant plasmids and validation by Sanger sequencing. **(D–F)** Co-IP assays using **(D)** anti-O-GlcNAc and **(E, F)** anti-Flag antibodies to detect the O-GlcNAcylation of WT RIPK1 versus S331A mutant in HaCaT cells. **(G)** A co-IP assay was performed to validate the potential O-GlcNAcylation sites of RIPK1 after OSMI-1 and TMG treatment. **(H)** Western blot validation of a custom Ser331 O-GlcNAc-specific antibody in HaCaT and OGT-KO cells. (**I)** Co-IP confirming OGT-mediated O-GlcNAcylation of RIPK1 at Ser331. **(J–K)** Co-IP results showing that OGT overexpression reduces RIPK1–RIPK3 complex formation and RIPK1 phosphorylation. **(L–M)** The interactions between $RIPK1^{WT}$ or $RIPK1^{S331A}$ and RIPK3 determined by Co-IP. Data represent three independent experiments.

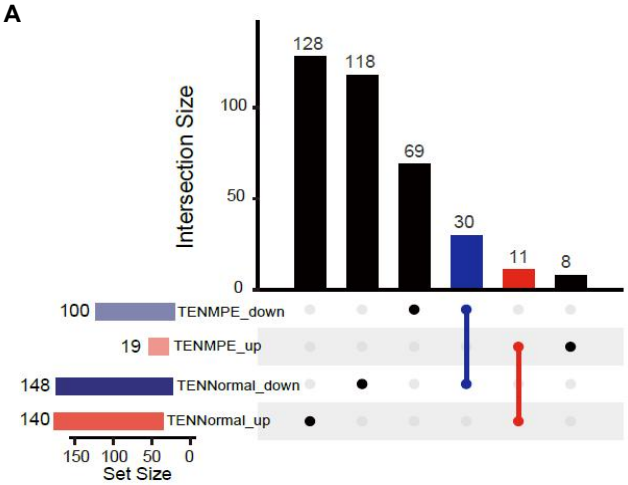
Fig. 6 RIPK1 O-GlcNAcylation at Ser331 regulates the formation of the FADD/Caspase-8 complex and K63-linked ubiquitination. Co-IP assays showing that **(A)** OSMI-1 treatment and **(B)** OGT-KO or **(C)** $RIPK1^{S331A}$ expression reduce RIPK1/FADD/Caspase-8 complex formation. Co-IP confirming RIPK1 ubiquitination in **(D)** OSMI-1-treated and **(E)** OGT-KO cells or **(F)** a dose-dependent increase in OGT-overexpressing cells. **(G)** Co-IP demonstrating the reduced ubiquitination of RIPK1 S331A versus WT. **(H–I)** Co-IP using K63- and K48-specific ubiquitin antibodies showing that **(H)** OSMI-1/OGT-KO and **(I)** RIPK1 S331A specifically reduce RIPK1 K63-linked ubiquitination. **(J)** Co-IP results showing the reduced ubiquitination of RIPK1 K377R versus WT. **(K)** Schematic representation of the predicted K63 ubiquitination sites in the RIPK1 ID. **(L)** Exogenous ubiquitination assays of lysine residue mutants of RIPK1 in HaCaT cells. Data are representative of three independent experiments.

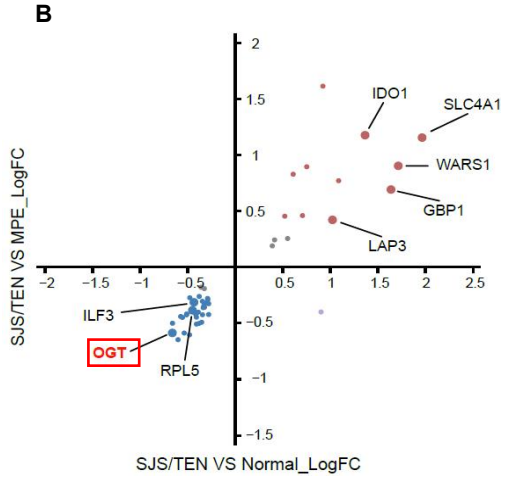
Fig. 7 RIPK1 O-GlcNAcylation at Ser331 suppresses the ID-mediated RIPK1–RIPK3 interaction and kinase activation. (A) Schematic of the RIPK1 domain architecture: kinase domain (KD), intermediate domain (ID), RIP homotypic interaction motif (RHIM), and death domain (DD). **(B)** RIPK1 serine 331 is highly conserved in mammals. **(C)** Western blots showing the levels of p-RIPK1 and p-MLKL in cells expressing RIPK1 WT or RIPK1 S331A. **(D–F)** Co-IP assays

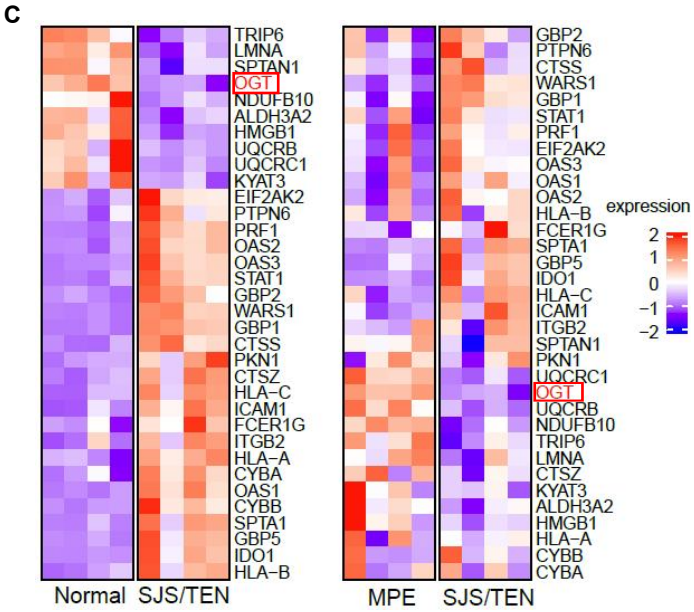
showing that WT OGT, but not K908A/H508A, inhibits RIPK1–RIPK3 binding and RIPK1 phosphorylation **(D–E)**; this effect is abrogated in RIPK1 S331A-expressing cells **(F)**. **(G)** Schematic representation of RIPK1 deletion mutants (ΔDI, ΔKI, and ΔD). **(H–J)** Immunoprecipitation with anti-FLAG **(H and J)** and anti-GFP **(I)** antibodies followed by immunoblotting for O-GlcNAc, p-RIPK1 or RIPK3. Data are representative of three independent experiments.

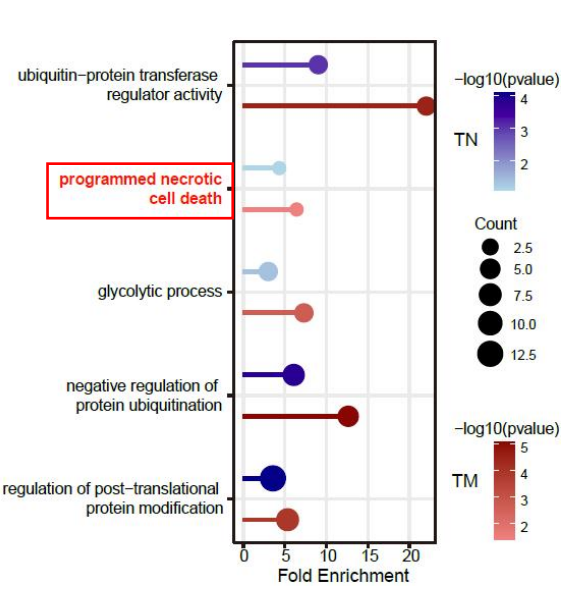
Fig. 8 O-GlcNAcase inhibition alleviates TEN severity *in vivo* and improves metabolic parameters. (A–J) C57BL/6J mice were treated with OSMI-1 (1 mg/kg), TMG (20 mg/kg), or PugNAc (10 mg/kg) before SM164-induced TEN; n = 7 mice per group. **(A)** Clinical assessment. **(B)** Histology. **(C)** Changes in body weight. **(D)** Lesion size. **(E)** Clinical score. **(F–G)** The expression of necroptosis-related proteins were analyzed using ELISA and **(H)** western blotting. **(I)** Spleen weight relative to body weight. **(J)** Serum levels of LDH, ALT, AST, and CK-MB. $*P < 0.05$, $**P < 0.01$, and $***P < 0.001$.

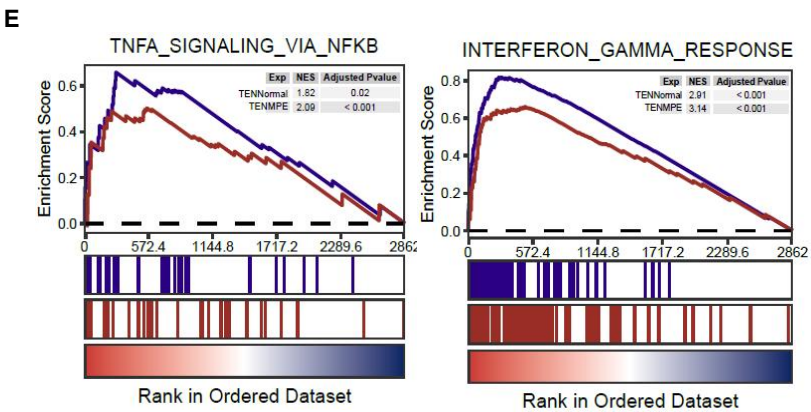
Fig. 9 Proposed model of RIPK1 O-GlcNAcylation at Ser331 in SJS/TEN pathogenesis. Schematic summarizing how nucleolar stress and impaired glucose metabolism triggers the OGT-mediated O-GlcNAcylation of RIPK1 at Ser331 and regulates keratinocyte necroptosis in individuals with SJS/TEN (Sensitizing drugs trigger immune cell activation and a massive inflammatory cytokine storm with abundant TNF-α release. This cascade impairs epidermal glucose uptake, HBP activity, and nucleolar stress consequently reducing OGT abundance. Downregulated OGT further diminishes O-GlcNAcylation of RIPK1 at Ser331 residue, removing the protective molecular "brake" imposed by this glycosylation modification on RIPK1. Loss of Ser331 O-GlcNAcylation attenuates K63-linked ubiquitination of RIPK1 and disrupts assembly of the cytoprotective RIPK1/FADD/Caspase-8 complex, while simultaneously boosting formation of the CYLD/RIPK1/cIAP2 complex. These molecular alterations facilitate necrosome assembly, activate necroptotic signaling in keratinocytes, and ultimately drive the progression of SJS/TEN lesions).

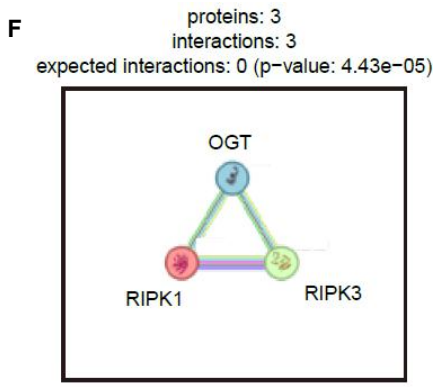

A
Intersection Size
128
118
69
30
11
8
100
50
0
100 TENMPE_down
19 TENMPE_up
148 TENNormal_down
140 TENNormal_up
150 100 50 0
Set Size

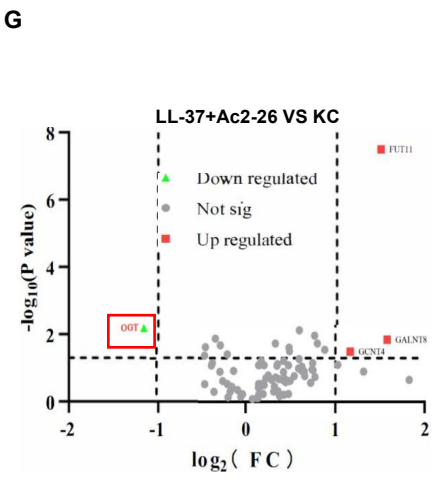

B
IDO1
SLC4A1
WARS1
GBP1
LAP3
ILF3
OGT
RPL5
SJS/TEN VS MPE_LogFC
SJS/TEN VS Normal_LogFC

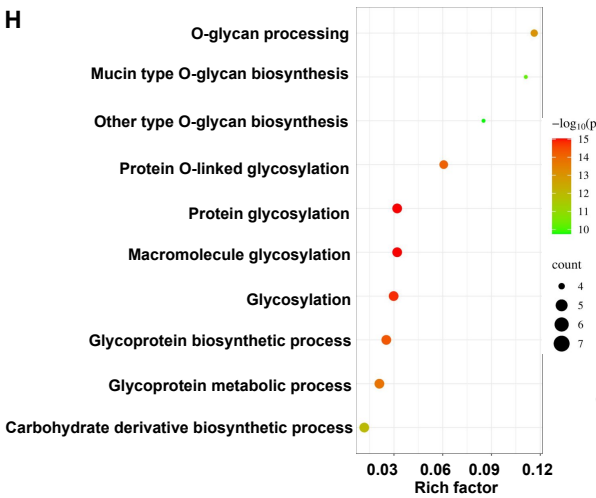

C
TRIP6
LMNA
SPTAN1
OGT
NDUFB10
ALDH3A2
HMGB1
UQCRB
UQCRC1
KYAT3
EIF2AK2
PTPN6
PRF1
OAS2
OAS3
STAT1
GBP2
WARS1
GBP1
CTSS
PKN1
CTSZ
HLA−C
ICAM1
FCER1G
ITGB2
HLA−A
CYBA
OAS1
CYBB
SPTA1
GBP5
IDO1
HLA−B
GBP2
PTPN6
CTSS
WARS1
GBP1
STAT1
PRF1
EIF2AK2
OAS3
OAS1
OAS2
HLA−B
FCER1G
SPTA1
GBP5
IDO1
HLA−C
ICAM1
ITGB2
SPTAN1
PKN1
UQCRC1
OGT
UQCRB
NDUFB10
TRIP6
LMNA
CTSZ
KYAT3
ALDH3A2
HMGB1
HLA−A
CYBB
CYBA
expression
2
1
0
−1
−2
Normal SJS/TEN
MPE SJS/TEN

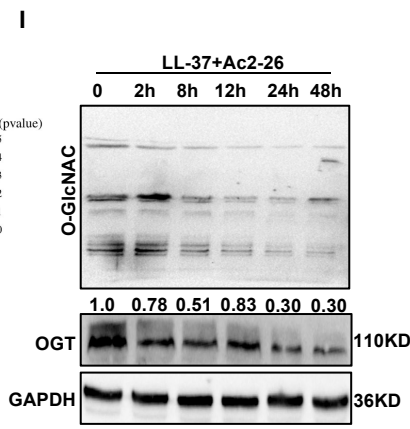

D
ubiquitin−protein transferase regulator activity
programmed necrotic cell death
glycolytic process
negative regulation of protein ubiquitination
regulation of post−translational protein modification
−log10(pvalue)
TN
Count
2.5
5.0
7.5
10.0
12.5
−log10(pvalue)
TM
0 5 10 15 20
Fold Enrichment

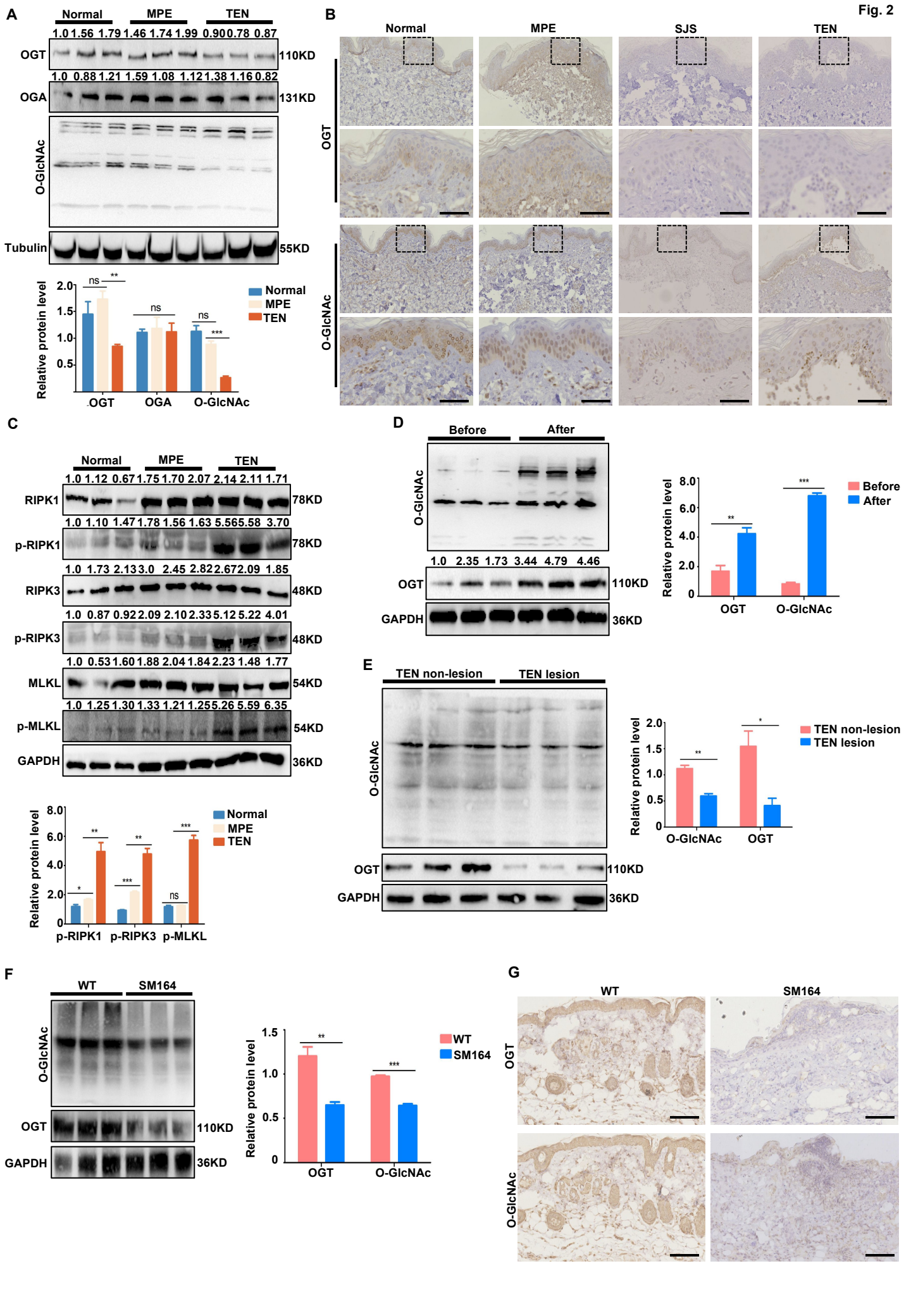

E
TNFA_SIGNALING_VIA_NFKB
INTERFERON_GAMMA_RESPONSE
Enrichment Score
Exp NES Adjusted Pvalue
TENNormal 1.82 0.02
TENMPE 2.09 < 0.001
TENNormal 2.91 < 0.001
TENMPE 3.14 < 0.001
0 572.4 1144.8 1717.2 2289.6 2862
Rank in Ordered Dataset

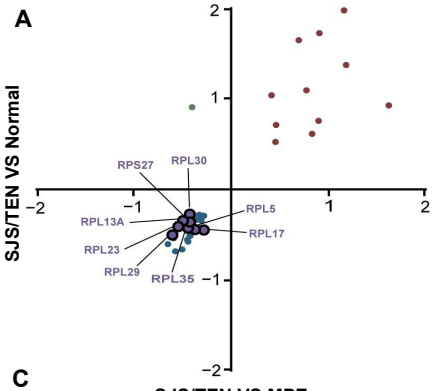

F
proteins: 3
interactions: 3
expected interactions: 0 (p−value: 4.43e−05)
OGT
RIPK1
RIPK3

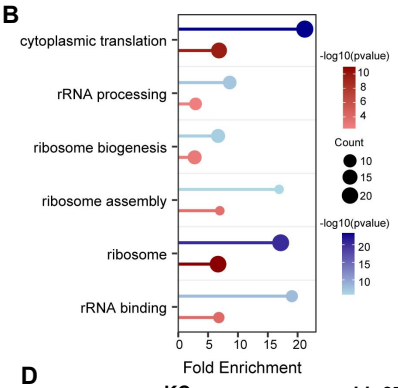

G
LL-37+Ac2-26 VS KC
Down regulated
Not sig
Up regulated
FUT11
OGT
GALNT8
GCNT4
−log10(P value)
log2(FC)

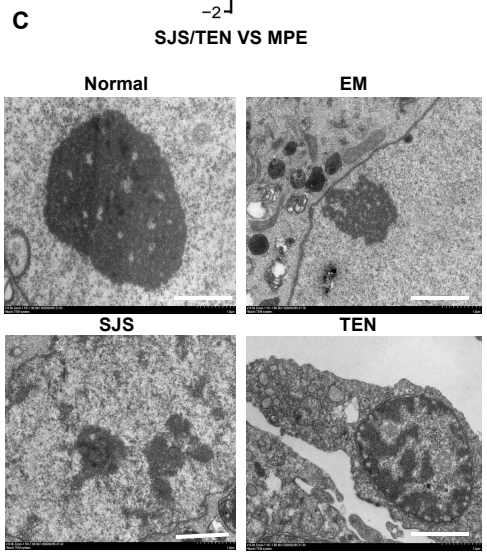

H
O-glycan processing
Mucin type O-glycan biosynthesis
Other type O-glycan biosynthesis
Protein O-linked glycosylation
Protein glycosylation
Macromolecule glycosylation
Glycosylation
Glycoprotein biosynthetic process
Glycoprotein metabolic process
Carbohydrate derivative biosynthetic process
−log10(pvalue)
count
0.03 0.06 0.09 0.12
Rich factor

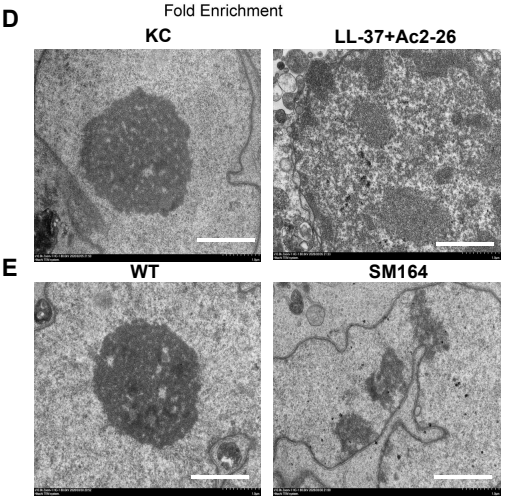

I
LL-37+Ac2-26
0 2h 8h 12h 24h 48h
O-GlcNAC
1.0 0.78 0.51 0.83 0.30 0.30
OGT
110KD
GAPDH
36KD

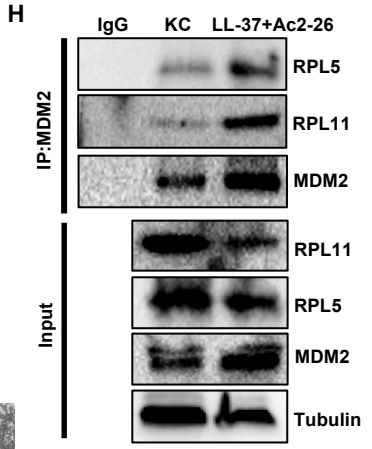

A
Normal
MPE
TEN
1.0 1.56 1.79 1.46 1.74 1.99 0.90 0.78 0.87
OGT
110KD
1.0 0.88 1.21 1.59 1.08 1.12 1.38 1.16 0.82
OGA
131KD
O-GlcNAc
Tubulin
55KD
Relative protein level
ns
**
ns
ns
***
Normal
MPE
TEN
OGT
OGA
O-GlcNAc
B
Normal
MPE
SJS
TEN
OGT
O-GlcNAc
C
Normal
MPE
TEN
1.0 1.12 0.67 1.75 1.70 2.07 2.14 2.11 1.71
RIPK1
78KD
1.0 1.10 1.47 1.78 1.56 1.63 5.56 5.58 3.70
p-RIPK1
78KD
1.0 1.73 2.13 3.0 2.45 2.82 2.67 2.09 1.85
RIPK3
48KD
1.0 0.87 0.92 2.09 2.10 2.33 5.12 5.22 4.01
p-RIPK3
48KD
1.0 0.53 1.60 1.88 2.04 1.84 2.23 1.48 1.77
MLKL
54KD
1.0 1.25 1.30 1.33 1.21 1.25 5.26 5.59 6.35
p-MLKL
54KD
GAPDH
36KD
Relative protein level
Normal
MPE
TEN
p-RIPK1
p-RIPK3
p-MLKL
D
Before
After
O-GlcNAc
1.0 2.35 1.73 3.44 4.79 4.46
OGT
110KD
GAPDH
36KD
Relative protein level
Before
After
OGT
O-GlcNAc
E
TEN non-lesion
TEN lesion
O-GlcNAc
OGT
110KD
GAPDH
36KD
Relative protein level
TEN non-lesion
TEN lesion
O-GlcNAc
OGT
F
WT
SM164
O-GlcNAc
OGT
110KD
GAPDH
36KD
Relative protein level
WT
SM164
OGT
O-GlcNAc
G
WT
SM164
OGT
O-GlcNAc

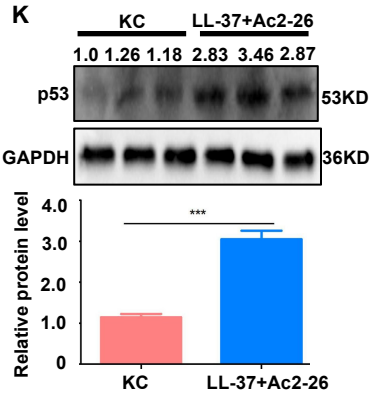

A
SJS/TEN VS Normal
SJS/TEN VS MPE
RPS27
RPL30
RPL5
RPL13A
RPL17
RPL23
RPL29
RPL35

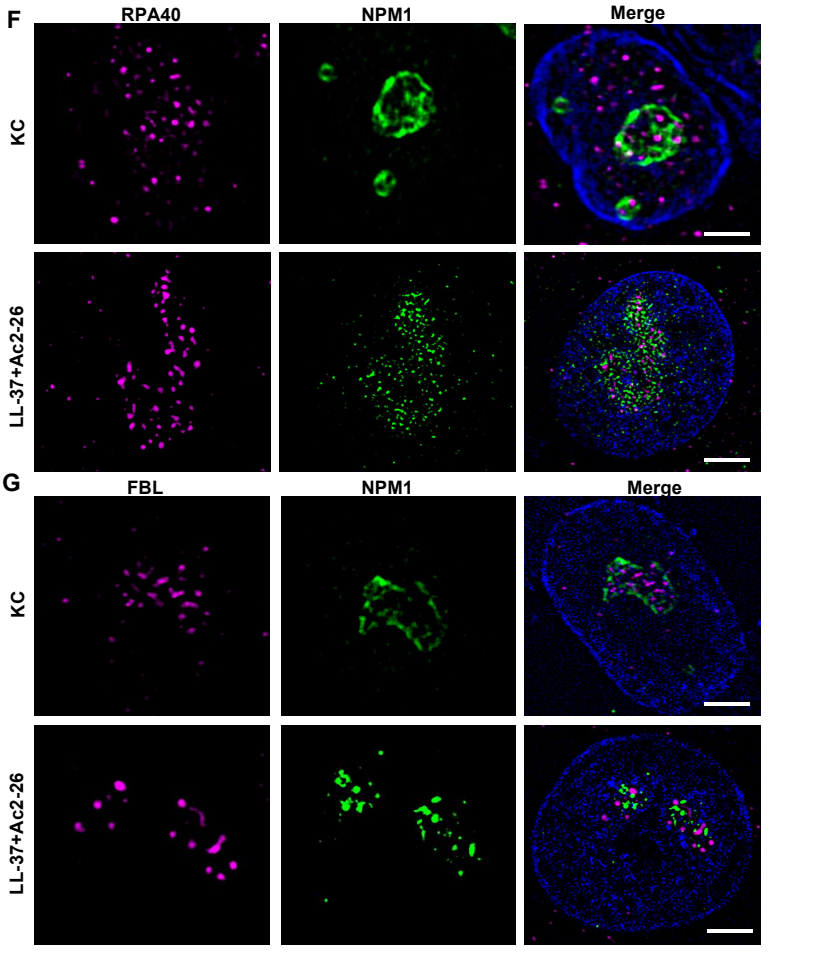

B
cytoplasmic translation
rRNA processing
ribosome biogenesis
ribosome assembly
ribosome
rRNA binding
-log10(pvalue)
Count
Fold Enrichment

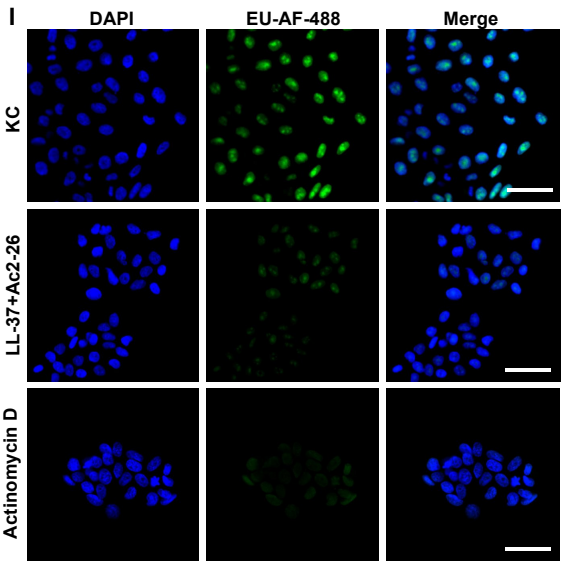

C
Normal
EM
SJS
TEN

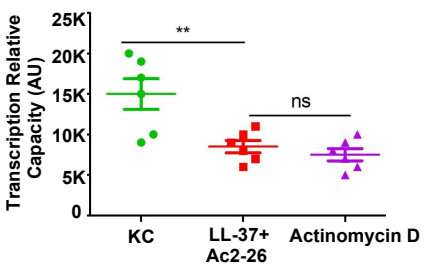

D
KC
LL-37+Ac2-26
E
WT
SM164

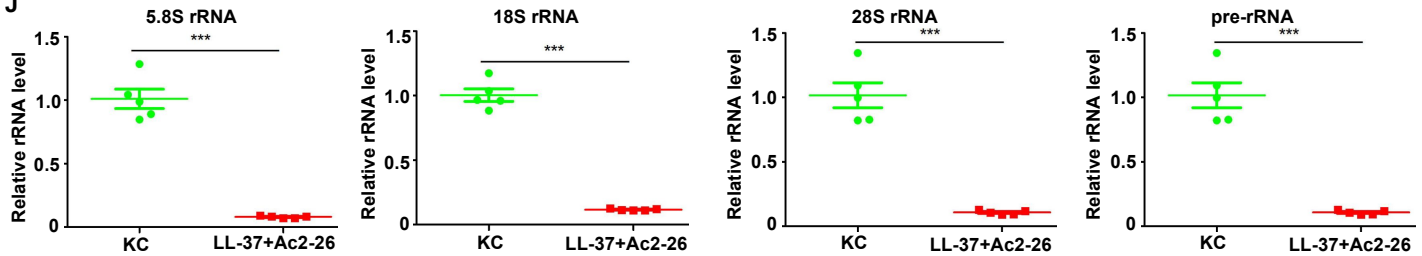

H
IgG
KC
LL-37+Ac2-26
IP:MDM2
RPL5
RPL11
MDM2
Input
RPL11
RPL5
MDM2
Tubulin


K
KC
LL-37+Ac2-26
1.0 1.26 1.18 2.83 3.46 2.87
p53
53KD
GAPDH
36KD
Relative protein level
***


F
RPA40
NPM1
Merge
KC
LL-37+Ac2-26
G
FBL
NPM1
Merge
KC
LL-37+Ac2-26


I
DAPI
EU-AF-488
Merge
KC
LL-37+Ac2-26
Actinomycin D


Transcription Relative Capacity (AU)
**
ns
KC
LL-37+ Ac2-26
Actinomycin D


J
5.8S rRNA
18S rRNA
28S rRNA
pre-rRNA
Relative rRNA level
***
KC
LL-37+Ac2-26

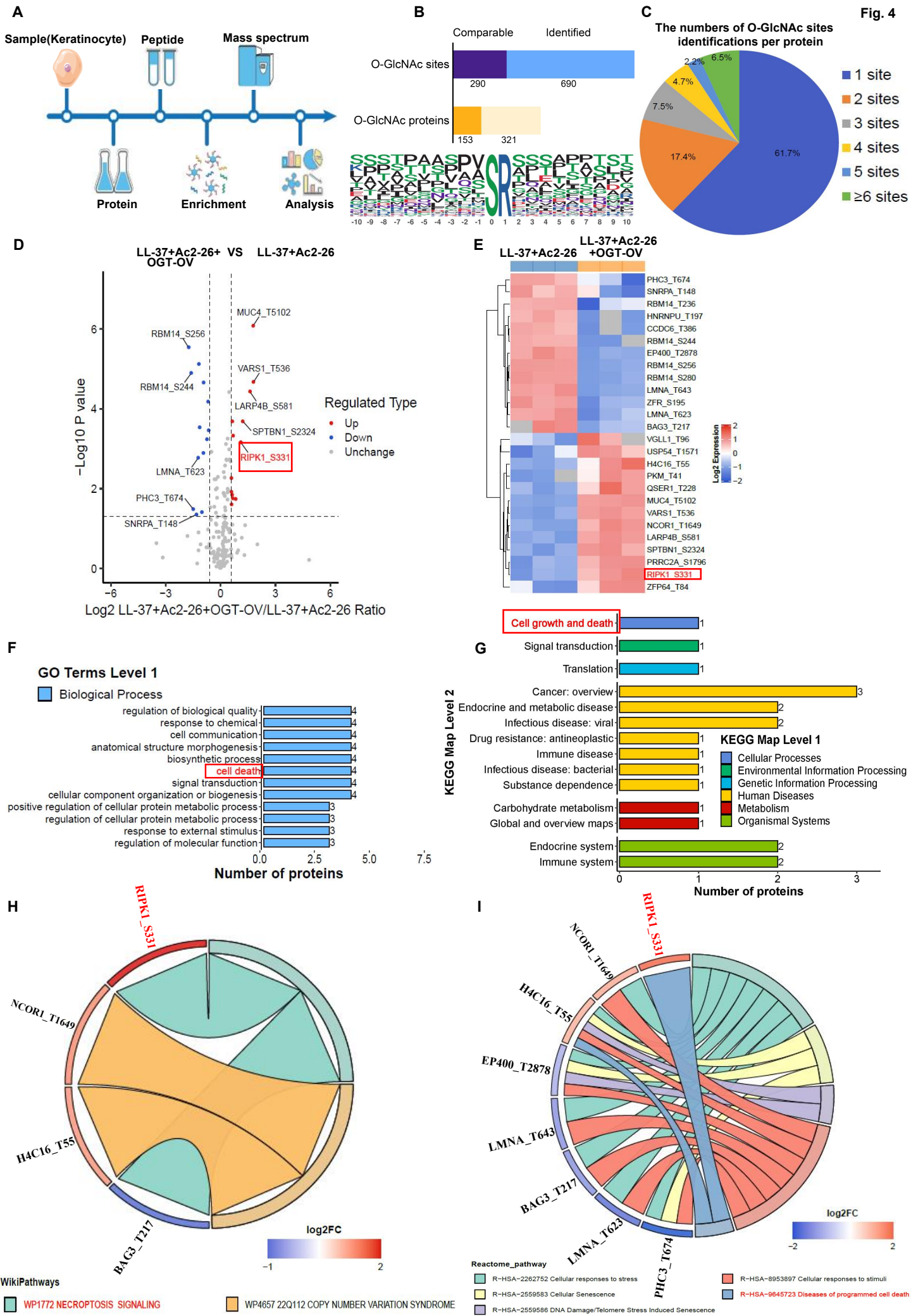
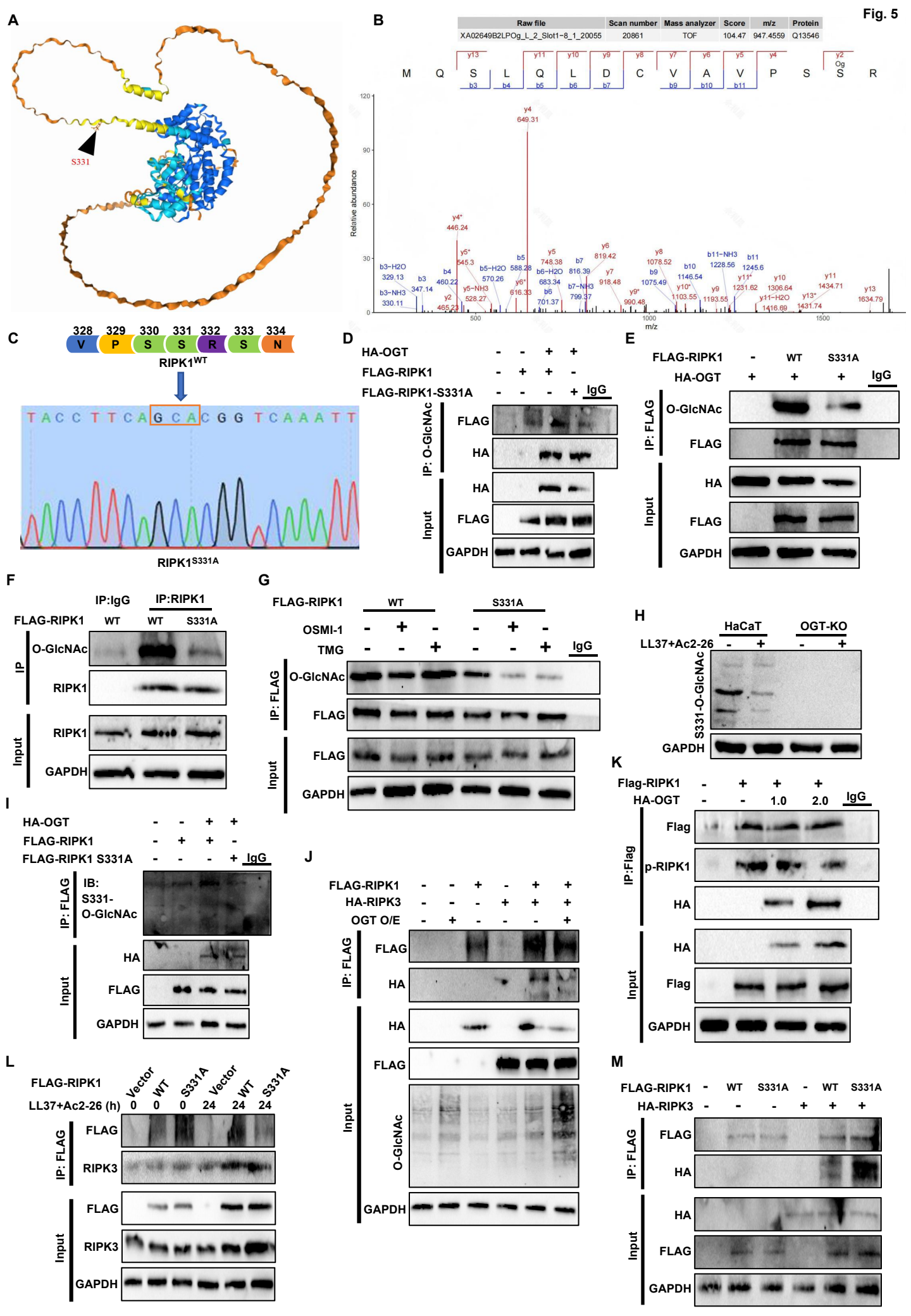
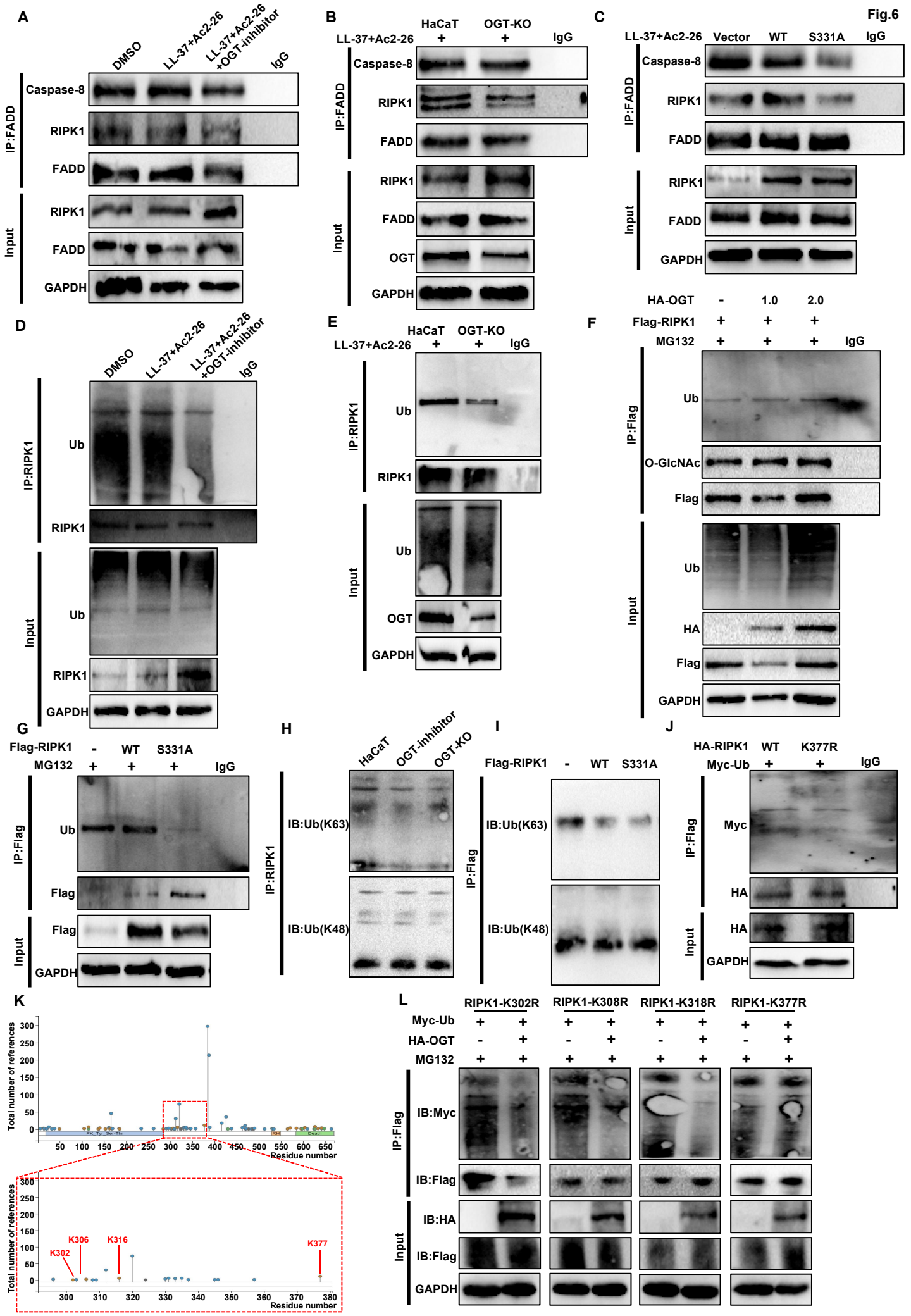
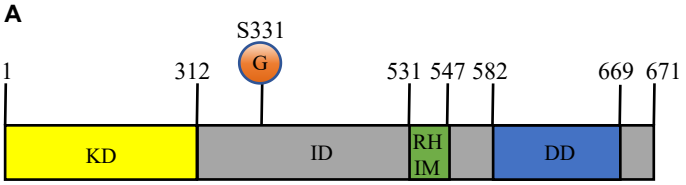

A
Sample(Keratinocyte)
Peptide
Mass spectrum
Protein
Enrichment
Analysis
B
Comparable
Identified
O-GlcNAc sites
290
690
O-GlcNAc proteins
153
321
C
The numbers of O-GlcNAc sites identifications per protein
1 site
2 sites
3 sites
4 sites
5 sites
≥6 sites
61.7%
17.4%
7.5%
4.7%
2.2%
6.5%
D
LL-37+Ac2-26+ OGT-OV VS LL-37+Ac2-26
MUC4_T5102
RBM14_S256
VARS1_T536
RBM14_S244
LARP4B_S581
SPTBN1_S2324
RIPK1_S331
LMNA_T623
PHC3_T674
SNRPA_T148
Regulated Type
Up
Down
Unchange
−Log10 P value
Log2 LL-37+Ac2-26+OGT-OV/LL-37+Ac2-26 Ratio
E
LL-37+Ac2-26
LL-37+Ac2-26 +OGT-OV
PHC3_T674
SNRPA_T148
RBM14_T236
HNRNPU_T197
CCDC6_T386
RBM14_S244
EP400_T2878
RBM14_S256
RBM14_S280
LMNA_T643
ZFR_S195
LMNA_T623
BAG3_T217
VGLL1_T96
USP54_T1571
H4C16_T55
PKM_T41
QSER1_T228
MUC4_T5102
VARS1_T536
NCOR1_T1649
LARP4B_S581
SPTBN1_S2324
PRRC2A_S1796
RIPK1_S331
ZFP64_T84
Log2 Expression
F
GO Terms Level 1
Biological Process
regulation of biological quality
response to chemical
cell communication
anatomical structure morphogenesis
biosynthetic process
cell death
signal transduction
cellular component organization or biogenesis
positive regulation of cellular protein metabolic process
regulation of cellular protein metabolic process
response to external stimulus
regulation of molecular function
Number of proteins
G
Cell growth and death
Signal transduction
Translation
Cancer: overview
Endocrine and metabolic disease
Infectious disease: viral
Drug resistance: antineoplastic
Immune disease
Infectious disease: bacterial
Substance dependence
Carbohydrate metabolism
Global and overview maps
Endocrine system
Immune system
KEGG Map Level 2
KEGG Map Level 1
Cellular Processes
Environmental Information Processing
Genetic Information Processing
Human Diseases
Metabolism
Organismal Systems
Number of proteins
H
RIPK1_S331
NCOR1_T1649
H4C16_T55
BAG3_T217
log2FC
WikiPathways
WP1772 NECROPTOSIS SIGNALING
WP4657 22Q112 COPY NUMBER VARIATION SYNDROME
I
RIPK1_S331
NCOR1_T1649
H4C16_T55
EP400_T2878
LMNA_T643
BAG3_T217
LMNA_T623
PHC3_T674
log2FC
Reactome_pathway
R-HSA-2262752 Cellular responses to stress
R-HSA-2559583 Cellular Senescence
R-HSA-2559586 DNA Damage/Telomere Stress Induced Senescence
R-HSA-8953897 Cellular responses to stimuli
R-HSA-9645723 Diseases of programmed cell death

Fig. 5

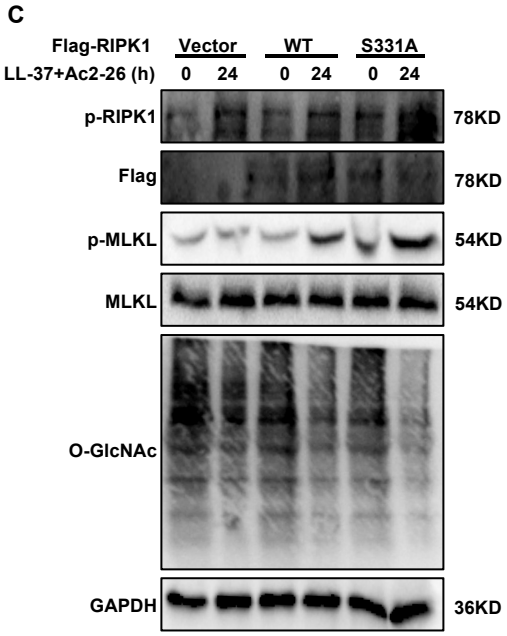

A
S331
B
Raw file
Scan number
Mass analyzer
Score
m/z
Protein
XA02649B2LPOg_L_2_Slot1-8_1_20055
20861
TOF
104.47
947.4559
Q13546
M Q S L Q L D C V A V P S S R
Relative abundance
m/z
C
328 329 330 331 332 333 334
V P S S R S N
RIPK1WT
T A C C T T C A G C A C G G T C A A A T T
RIPK1S331A
D
HA-OGT
FLAG-RIPK1
FLAG-RIPK1-S331A
IgG
IP: O-GlcNAc
FLAG
HA
Input
HA
FLAG
GAPDH
E
FLAG-RIPK1
WT
S331A
HA-OGT
IgG
IP: FLAG
O-GlcNAc
FLAG
Input
HA
FLAG
GAPDH
F
IP:IgG
IP:RIPK1
FLAG-RIPK1
WT
WT
S331A
IP
O-GlcNAc
RIPK1
Input
RIPK1
GAPDH
G
FLAG-RIPK1
WT
S331A
OSMI-1
TMG
IgG
IP: FLAG
O-GlcNAc
FLAG
Input
FLAG
GAPDH
H
HaCaT
OGT-KO
LL37+Ac2-26
S331-O-GlcNAc
GAPDH
I
HA-OGT
FLAG-RIPK1
FLAG-RIPK1 S331A
IgG
IP: FLAG
IB:
S331-
O-GlcNAc
Input
HA
FLAG
GAPDH
J
FLAG-RIPK1
HA-RIPK3
OGT O/E
IP: FLAG
FLAG
HA
Input
HA
FLAG
O-GlcNAc
GAPDH
K
Flag-RIPK1
HA-OGT
1.0
2.0
IgG
IP:Flag
Flag
p-RIPK1
HA
Input
HA
Flag
GAPDH
L
FLAG-RIPK1
Vector
WT
S331A
Vector
WT
S331A
LL37+Ac2-26 (h)
0 0 0 24 24 24
IP: FLAG
FLAG
RIPK3
Input
FLAG
RIPK3
GAPDH
M
FLAG-RIPK1
WT
S331A
WT
S331A
HA-RIPK3
IP: FLAG
FLAG
HA
Input
HA
FLAG
GAPDH

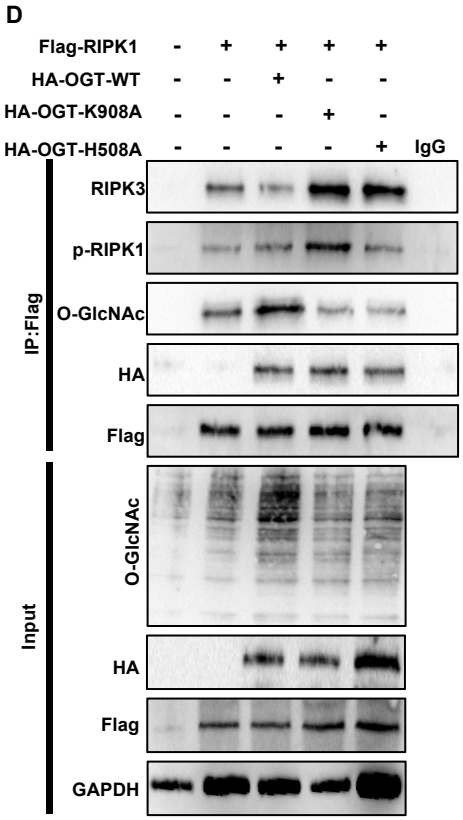

A
DMSO
LL-37+Ac2-26
LL-37+Ac2-26 +OGT-inhibitor
IgG
IP:FADD
Caspase-8
RIPK1
FADD
Input
RIPK1
FADD
GAPDH
B
HaCaT
OGT-KO
LL-37+Ac2-26
IgG
IP:FADD
Caspase-8
RIPK1
FADD
Input
RIPK1
FADD
OGT
GAPDH
C
LL-37+Ac2-26
Vector
WT
S331A
IgG
IP:FADD
Caspase-8
RIPK1
FADD
Input
RIPK1
FADD
GAPDH
D
DMSO
LL-37+Ac2-26
LL-37+Ac2-26 +OGT-inhibitor
IgG
IP:RIPK1
Ub
RIPK1
Input
Ub
RIPK1
GAPDH
E
HaCaT
OGT-KO
LL-37+Ac2-26
IgG
IP:RIPK1
Ub
RIPK1
Input
Ub
OGT
GAPDH
F
HA-OGT
-
1.0
2.0
Flag-RIPK1
MG132
IgG
IP:Flag
Ub
O-GlcNAc
Flag
Input
Ub
HA
Flag
GAPDH
G
Flag-RIPK1
-
WT
S331A
MG132
IgG
IP:Flag
Ub
Flag
Input
Flag
GAPDH
H
HaCaT
OGT-inhibitor
OGT-KO
IP:RIPK1
IB:Ub(K63)
IB:Ub(K48)
I
Flag-RIPK1
-
WT
S331A
IP:Flag
IB:Ub(K63)
IB:Ub(K48)
J
HA-RIPK1
WT
K377R
Myc-Ub
IgG
IP:Flag
Myc
HA
Input
HA
GAPDH
K
Total number of references
Residue number
K302
K306
K316
K377
L
RIPK1-K302R
RIPK1-K308R
RIPK1-K318R
RIPK1-K377R
Myc-Ub
HA-OGT
MG132
IP:Flag
IB:Myc
IB:Flag
Input
IB:HA
IB:Flag
GAPDH

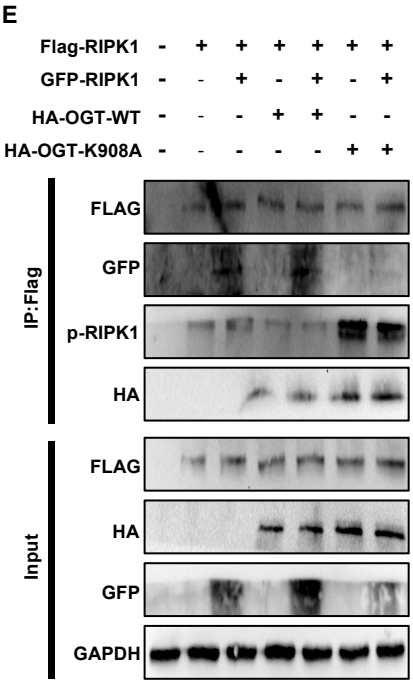


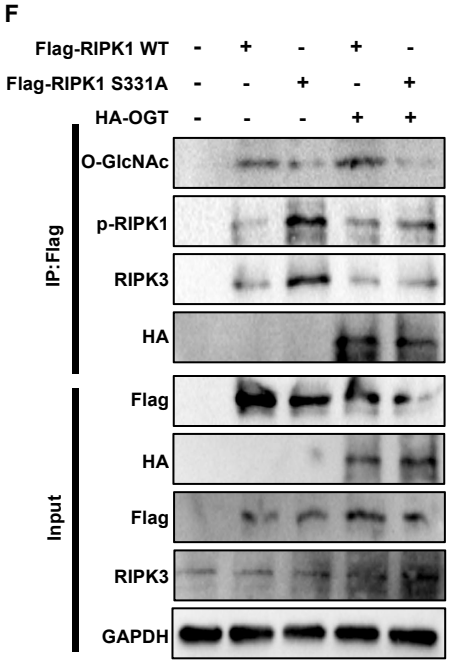
B

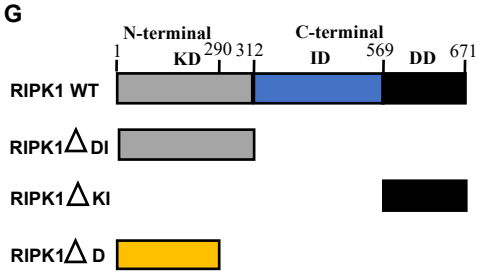
Homo sapiens	325	CVAVPS **S** RSN
Pan troglodytes	325	CVAVPS **S** RSN
Mus musculus	326	CVPLPP **S** RSN
Rattus norvegicus	325	CVPLPP **S** RSN
Ovibos moschatus	321	CVAIAP **S** RSN
Lepus granatensis	321	CVPAPP **S** RSN
Canis lupus baileyi	323	CVATPP **S** RSN

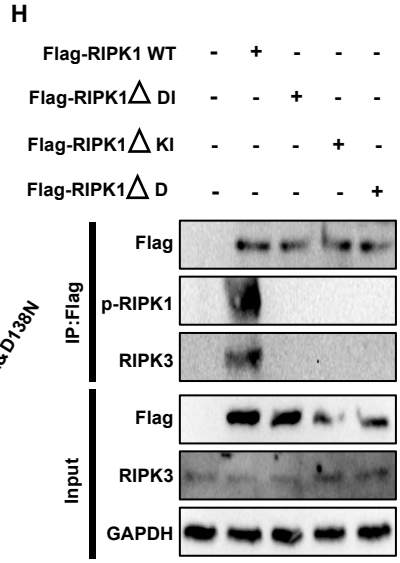


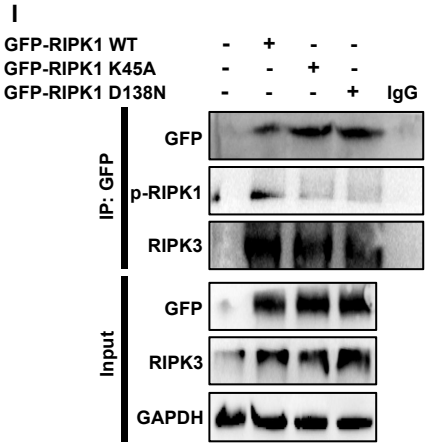


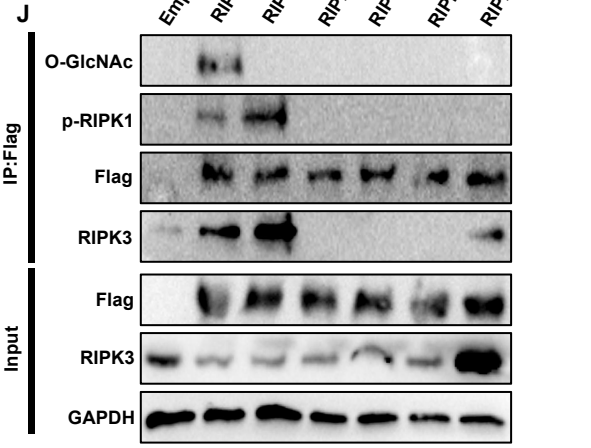


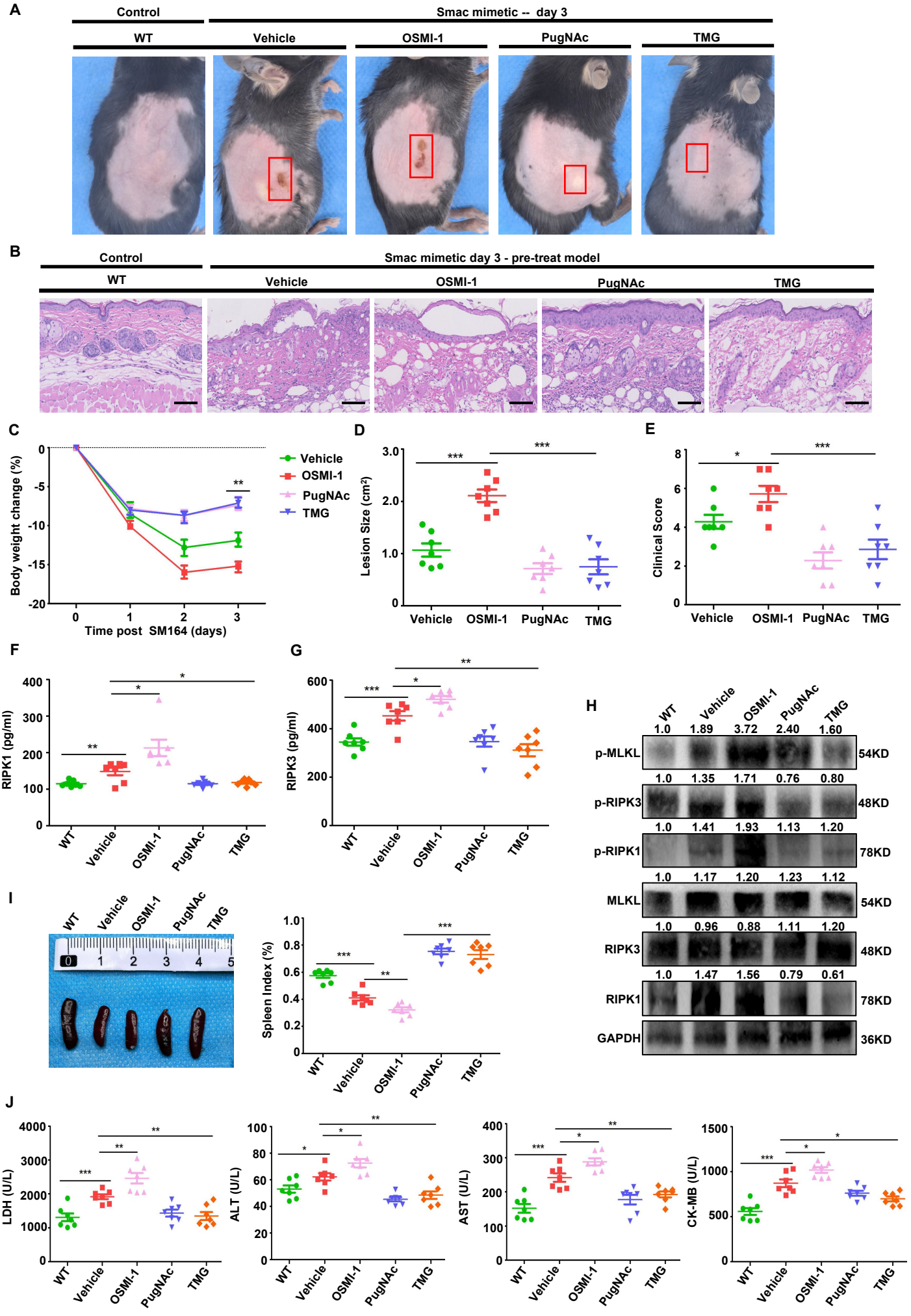


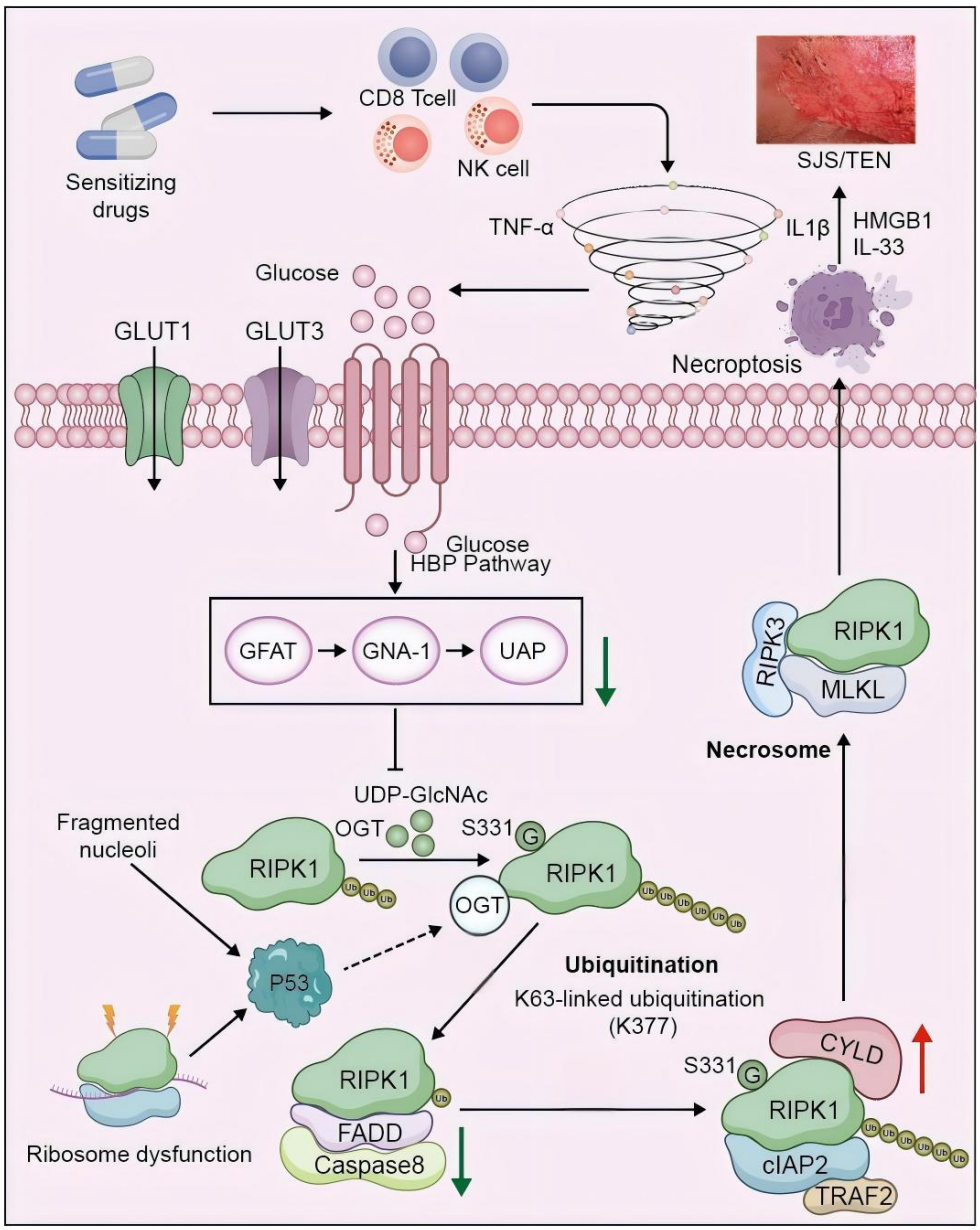









A
Control
Smac mimetic -- day 3
WT
Vehicle
OSMI-1
PugNAc
TMG
B
Control
Smac mimetic day 3 - pre-treat model
WT
Vehicle
OSMI-1
PugNAc
TMG
C
Body weight change (%)
Time post SM164 (days)
Vehicle
OSMI-1
PugNAc
TMG
D
Lesion Size (cm²)
E
Clinical Score
F
RIPK1 (pg/ml)
G
RIPK3 (pg/ml)
H
p-MLKL
p-RIPK3
p-RIPK1
MLKL
RIPK3
RIPK1
GAPDH
54KD
48KD
78KD
54KD
48KD
78KD
36KD
I
Spleen Index (%)
J
LDH (U/L)
ALT (U/L)
AST (U/L)
CK-MB (U/L)


Sensitizing drugs
CD8 Tcell
NK cell
SJS/TEN
TNF-α
IL1β
HMGB1
IL-33
Glucose
GLUT1
GLUT3
Necroptosis
Glucose
HBP Pathway
GFAT
GNA-1
UAP
RIPK3
RIPK1
MLKL
Necrosome
UDP-GlcNAc
Fragmented nucleoli
OGT
S331
G
RIPK1
OGT
RIPK1
P53
Ubiquitination
K63-linked ubiquitination (K377)
CYLD
S331
G
RIPK1
FADD
Caspase8
cIAP2
TRAF2
Ribosome dysfunction

Supplementary Files

This is a list of supplementary files associated with this preprint. Click to download.

- CDDSupplementarymaterial.pdf
- SupplementaryTableCDD.docx
- WB.pdf